RESEARCH ARTICLE

Allelic compatibility in plant immune receptors facilitates engineering of new effector recognition specificities

Adam R. Bentham[1]*, Juan Carlos De la Concepcion[1,2]*, Javier Vega Benjumea[1,3], Jiorgos Kourelis[4], Sally Jones[1], Melanie Mendel[1,5], Jack Stubbs[1,6,7], Clare E. M. Stevenson[1], Josephine H.R. Maidment[1,4,8], Mark Youles[4], Rafał Zdrzałek[1], Sophien Kamoun[4], Mark J. Banfield[1#]

[1] Department of Biochemistry and Metabolism, John Innes Centre, Norwich Research Park, Norwich, NR4 7UH, UK

[2] Current address: Gregor Mendel Institute of Molecular Plant Biology, Austrian Academy of Sciences, Vienna, 1030, Austria

[3] Current address: Servicio de bioquímica y análisis clínicos, Hospital Universitario Puerta de Hierro, Majadahonda, 28222, Spain

[4] The Sainsbury Laboratory, University of East Anglia, Norwich Research Park, Norwich, NR4 7UH, UK

[5] Current address: Department of Biology, Plant-Microbe Interactions, Utrecht University, 3584CH, Utrecht, The Netherlands

[6] Current address: Biological Sciences, Institute for Life Sciences, University of Southampton, Hartley Library B12, University Rd, Highfield, Southampton SO17 1BJ, UK

[7] Current address: Diamond Light Source, Harwell Science and Innovation Campus, Fermi Ave, Didcot OX11 0DE, UK

[8] Current affiliation: 2Blades, Evanston, IL 60201, USA

* These authors contributed equally.

Corresponding author: Mark J. Banfield, mark.banfield@jic.ac.uk

ORCID IDs

Adam R. Bentham: 0000-0001-5906-0962
Juan Carlos De la Concepcion: 0000-0002-7642-8375
Javier Vega Benjumea: 0000-0002-3988-1656
Jiorgos Kourelis: 0000-0002-9007-1333
Sally Jones: 0000-0002-0013-8865
Melanie Mendel: 0000-0003-2409-7479

Jack Stubbs: 0000-0002-3788-1687
Clare E. M. Stevenson: 0000-0001-6695-8201
Josephine H.R. Maidment: 0000-0002-8229-2718
Mark Youles: 0000-0003-2953-7533
Rafał Zdrzałek: 0000-0003-3669-924X
Sophien Kamoun: 0000-0002-0290-0315
Mark J. Banfield: 0000-0001-8921-3835

Short title: Engineering NLR immune receptors

The author responsible for distribution of materials integral to the findings presented in this article in accordance with the policy described in the Instructions for Authors (https://academic.oup.com/plcell/pages/General-Instructions) is: Mark J Banfield (mark.banfield@jic.ac.uk).

Abstract

Engineering the plant immune system offers genetic solutions to mitigate crop diseases caused by diverse agriculturally significant pathogens and pests. Modification of intracellular plant immune receptors of the nucleotide-binding leucine rich repeat (NLR) superfamily for expanded recognition of pathogen virulence proteins (effectors) is a promising approach for engineering disease resistance. However, engineering can cause NLR autoactivation, resulting in constitutive defence responses that are deleterious to the plant. This may be due to plant NLRs associating in highly complex signalling networks that co-evolve together, and changes through breeding or genetic modification can generate incompatible combinations, resulting in autoimmune phenotypes. The sensor and helper NLRs of the rice (*Oryza sativa*) NLR pair Pik have co-evolved, and mismatching between non-co-evolved alleles triggers constitutive activation and cell death. This limits the extent to which protein modifications can be used to engineer pathogen recognition and enhance disease resistance mediated by these NLRs. Here, we dissected incompatibility determinants in the Pik pair in *Nicotiana benthamiana* and found that heavy metal-associated (HMA) domains integrated in Pik-1 not only evolved to bind pathogen effectors but also likely co-evolved with other NLR domains to maintain immune homeostasis. This explains why changes in integrated domains can lead to autoactivation. We then used this knowledge to facilitate engineering of new effector recognition specificities, overcoming initial autoimmune penalties. We show that by mismatching alleles of the rice sensor and helper NLRs Pik-1 and Pik-2, we can enable the integration of synthetic domains with novel and enhanced recognition specificities. Taken together, our results reveal a strategy for engineering NLRs, which has the potential to allow an expanded set of integrations and therefore new disease resistance specificities in plants.

IN A NUTSHELL

Background: Plants use specialized intracellular immune receptors called nucleotide-binding leucine-rich repeat (NLR) to detect pathogen effector proteins secreted into the host during infection. Effectors aid plant colonization, which can result in serious disease and limit crop yields in agriculture. Therefore, immune responses triggered by NLRs upon perception of effectors are essential to maintain plants healthy. However, plant pathogens use hundreds of effectors during infection and these effectors evolve rapidly, escaping from recognition by NLR immune proteins. Recently, bioengineering of NLRs to recognize a wider range of effectors was demonstrated to be an effective means of generating disease resistant plants. However, bioengineering of NLRs can result in 'autoactivity' where the immune system is constantly active. This is deleterious to the health of the plant.

Question: In our study, we strived to understand the limits of bioengineering for a pair of rice NLRs called Pik. Pik are interesting NLRs as they comprise a sensor NLR (important for effector recognition) and a helper NLR (important for defense signaling). Findings: We found bioengineering of the native Pik sensor NLR often resulted in autoactivity. However, by using different combinations of Pik helper NLR alleles (an alternative form of the gene) we could mitigate the autoactivity caused by bioengineering, allowing us to generate Pik sensor NLRs with different effector recognition specificities in the model plant *Nicotiana benthamiana*. Our study establishes a strategy to incorporate a wider variety of effector recognition modules into the Pik NLRs without autoactivity.

Next Steps: The next step in this research is to understand whether this bioengineered resistance is transferable from model plants to stable transgenic crops, such as rice (*Oryza sativa*), barley (*Hordeum vulgare*), wheat (*Triticum aestivum*) or maize (*Zea mays*), and to

understand which pathogens are the best targets for new disease resistance using the Pik NLRs.

Introduction

Engineering the plant immune system is a promising genetic solution to prevent pathogen infection thereby reducing crop losses and global food insecurity caused by plant pathogens (Bentham et al., 2020; Outram et al., 2022). Nucleotide-binding leucine rich repeat receptors (NLRs) are intracellular immune proteins that trigger robust defence responses upon recognition of pathogen virulence proteins (effectors) delivered into the host during infection (Burdett et al., 2019; Jones et al., 2016). Effector recognition by NLRs often culminates in cell death that isolates the invading pathogen and confers resistance (Jones et al., 2016; Maruta et al., 2022). Due to their effective and specific responses to plant pathogens, engineering of NLRs to increase their effector recognition specificities is a promising approach to boost disease resistance (Marchal et al., 2022; Monteiro and Nishimura, 2018; Outram et al., 2022).

NLRs are typically modular tripartite proteins that consist of an N-terminal signalling domain, either a coiled-coil (CC) domain, a CC domain with homology to RPW8 (CC_R) or Toll-interleukin-1 receptor (TIR) domain, a central nucleotide-binding (NB) domain, and a C-terminal leucine rich repeat (LRR) domain (Jones et al., 2016; Lüdke et al., 2022; Takken and Goverse, 2012). NLR proteins can function as singletons, in pairs and in networks, and utilize several mechanisms to detect and respond to pathogen effectors (Adachi et al., 2019; Cesari, 2018; Wu et al., 2018). One such mechanism is the use of integrated domains, which function as effector baits embedded within the canonical NLR architecture (Baggs et al., 2017; Cesari et al., 2014). Integrated domains often share homology to pathogen host targets

and effector binding results in NLR activation (Białas et al., 2018; Cesari, 2018; Kroj et al., 2016; Sarris et al., 2016). Due to their role in effector recognition, integrated domains are key targets for engineering disease resistance in NLRs, and only a few mutations to these domains can lead to novel effector recognition profiles (Cesari et al., 2022; De la Concepcion et al., 2019; Liu et al., 2021; Maidment et al., 2022; Zhang et al., 2022).

Most characterised NLRs that contain integrated domains (NLR-IDs) are found as a part of a sensor/helper receptor pair, where the NLR-ID is referred to as the sensor, and its signalling partner, the helper (Adachi et al., 2019; Cesari, 2018; Feehan et al., 2020). Some of the best characterised examples of paired NLRs are the Arabidopsis (*Arabidopsis thaliana*) RRS1 (RESISTANCE TO *RALSTONIA SOLANACEARUM* 1) /RPS4 (RESISTANCE TO PSEUDOMONAS SYRINGAE 4) pair which encode an RRS1-integrated WRKY domain (Le Roux et al., 2015; Mukhi et al., 2021; Zhang et al., 2017) and the rice (*Oryza sativa*) NLR pairs RGA5/RGA4 and Pik-1/Pik-2 (Cesari et al., 2013; Kanzaki et al., 2012; Zdrzałek et al., 2020). The RGA5/RGA4 and Pik pairs harbour an integrated HMA domain in their sensor NLRs RGA5 and Pik-1 that directly bind and recognise MAX (*Magnaporthe oryzae* avirulence and ToxB-like) effectors (Guo et al., 2018; Maqbool et al., 2015). While both RGA5 and Pik-1 contain an integrated HMA domain, their domain architecture is distinct with the Pik-1 HMA domain located between the CC and NB domains, and the RGA5 HMA domain located at the C-terminus, after the LRR (Cesari et al., 2013; Kanzaki et al., 2012; Maqbool et al., 2015; Ortiz et al., 2017). Further, these HMA domains provide distinct effector recognition specificities for AVR-Pik, AVR-Mgk1, and AVR-Pia/AVR1-CO39 effectors respectively (Białas et al., 2018; Sugihara et al., 2022).

142 The HMA domains of Pik-1 and RGA5 use spatially distinct protein interfaces for effector
143 recognition (De la Concepcion et al., 2021a, 2018; Guo et al., 2018; Varden et al., 2019). Recent
144 studies have reported HMA domain engineering to be an effective way to generate new
145 resistance specificities for rice against the rice blast pathogen *M. oryzae*. In particular, three
146 separate studies have shown the RGA5 HMA domain can be engineered to recognise other
147 MAX effectors. One study showed engineered resistance to *M. oryzae* isolates carrying AVR-
148 Pib in rice (Liu et al., 2021), and two studies engineered recognition of AVR-Pik in *Nicotiana*
149 *benthamiana*, one of which was able to provide resistance in rice (Cesari et al., 2022; Zhang et
150 al., 2022). Extensive study of the Pik-1 HMA domain has also demonstrated this domain to
151 be amenable to engineering (De la Concepcion et al., 2021a, 2019; Maidment et al., 2022).
152 Recently, it has been shown the Pik-1 HMA can be substituted for VHH nanobody fusions
153 that act as synthetic effector recognition domains, demonstrating the flexibility of the Pik
154 system for mutation or substitution of new integrated domains (Kourelis et al., 2023).

155 Despite some success, plant immune receptor engineering remains challenging. NLRs exist
156 in complex, regulated systems and, as a consequence, some changes in NLRs that expand
157 recognition can also result in constitutive defence signalling that is deleterious for plant
158 growth (Białas et al., 2021; Maidment et al., 2022; Tamborski et al., 2023). In particular, the
159 manipulation of integrated domains in paired NLRs often results in autoactivity. This is best
160 exemplified by several studies of the Pik NLR pair, in which the integrated domain of the
161 Pik-1 sensor was substituted for an engineered variant or entirely different domains,
162 resulting in autoactivation of the receptor pair (Białas et al., 2021; Kourelis et al., 2023;
163 Maidment et al., 2022). NLR-mediated autoimmunity has been well documented, with
164 hybrid necrosis phenotypes as a result of crosses linked to incompatible pairing of NLRs
165 (Bomblies et al., 2007; Chae et al., 2014; Kourelis and Adachi, 2022; Tran et al., 2017),

166 presenting a bottleneck to producing new resistant crop varieties either by breeding or
167 precision protein engineering.

168 Recently, we demonstrated alleles of the rice Pik NLR pair have differentially co-evolved,
169 likely driven by their differences in recognition specificity for *M. oryzae* AVR-Pik effector
170 variants (De la Concepcion et al., 2021b). The Pik alleles Pikp and Pikm have undergone
171 functional diversification, with multiple changes in their integrated HMA domain that result
172 in different recognition specificities for AVR-Pik variants (Bialas et al., 2021; De la
173 Concepcion et al., 2021). Where the Pikp-1 sensor is restricted to detecting AVR-PikD, Pikm-
174 1 is able to recognise AVR-PikD, AVR-PikE and AVR-PikA (De la Concepcion et al., 2018;
175 Kanzaki et al., 2012). The helper NLRs Pikp-2 and Pikm-2 also appear to have undergone
176 diversification to match their sensor partners that results in a one-way incompatibility
177 between Pik alleles (De la Concepcion et al., 2021b). While Pikp-2 can be used as a helper
178 with Pikm-1 to recognise AVR-Pik effectors, the Pikp-1/Pikm-2 combination results in
179 constitutive cell death in *N. benthamiana*. This incompatibility between Pikp-1 and Pikm-2 is
180 linked to a single polymorphism in the NB-ARC of Pikm-2, which when mutated to the
181 equivalent residue of Pikp-2 reinstates compatibility (De la Concepcion et al., 2021b).

182 Here, we demonstrate the autoactivity triggered by the engineering of Pikm-1 for expanded
183 effector recognition capabilities can be attenuated by the co-expression with Pikp-2 without
184 compromising receptor function. For this, we delineate the basis for receptor incompatibility
185 between Pikp and Pikm alleles, describing Pikp-2 as a facilitator for integration of new
186 integrated domains into Pikm-1. By mismatching Pikm-1 with Pikp-2, we can integrate the
187 RGA5 HMA domain into Pikm-1, enabling further engineering of RGA5 HMA to recognise
188 multiple AVR-Pik effector variants. We structurally and biophysically characterise the

interaction between a synthetic AVR-Pik-binding mutant of RGA5 HMA and AVR-Pik effectors, highlighting the importance of binding affinity between effector and bait for immune recognition. As a final demonstration of the utility of helper mismatching, we demonstrate this strategy also allows for the integration of fluorescent protein (FP)-binding nanobodies into the Pikm-1 chassis without autoactivation, resulting in synthetic receptors capable of responding to eGFP or mCherry in planta. These results emphasize the importance of the immune receptor context when attempting NLR engineering, supplying an alternative approach to aid in the implementation of modified immune receptors with expanded effector recognition specificities outside of that previously observed in nature.

Results

The Pik-HMA domain is not required for effector-independent immune signalling.

Mismatched pairing of the Pikp-1/Pikm-2 alleles triggers constitutive cell death in the absence of an effector binding to the integrated HMA domain (De la Concepcion et al., 2021b). To better assess the role of the Pik HMA domain in signalling, activation and autoimmunity outside of effector binding, we used an HMA-absent Pikp-1 variant (Pikp-1$^{\Delta HMA}$) where the HMA domain of Pikp-1 was substituted with the unrelated NOI domain from the rice NLR Pii-2 (Pii-2 residues Glu1016 to Lys1052) (Fujisaki et al., 2017). Constitutive cell death was observed upon co-expression of Pikp-1$^{\Delta HMA}$ with Pikm-2 in *N. benthamiana*. However, like wildtype Pikp-1, co-expression of Pikp-1$^{\Delta HMA}$ with Pikp-2 did not result in cell death (**Figure 1 – Appendix 1A**).

The Pikp-2 and Pikm-2 helpers only differ by three polymorphisms: Asp230Glu, Thr434Ser and Met627Val. We made reciprocal mutants of Pikp-2 and Pikm-2 helpers for each of these polymorphisms, generating six mutants (Pikp-2^{D230E}, Pikp-2^{T434S}, Pikp-2^{M627V}; Pikm-2^{E230D}, Pikm-2^{S434T}, Pikm-2^{V627M}) and found autoactivity induced by co-expression of Pikp-1$^{\Delta HMA}$/Pikm-2 is determined by the Pik-2 Asp230Glu polymorphism (Pikp-2^{D230E}/Pikm-2^{E230D}) (**Figure 1 – Appendix 1A**) as previously described for wildtype Pik NLRs (De la Concepcion et al., 2021b). An Asp230Glu mutation into Pikp-2 resulted in constitutive activation when co-expressed with Pikp-1$^{\Delta HMA}$, and the reciprocal mutation, Glu230Asp, in Pikm-2 abolished autoactivity (**Figure 1 – Appendix 1A**). This suggests the integrated HMA domain acts as an effector binding domain but is not required for downstream NLR signalling and cell death.

Incompatibility between alleles of the Pik NLR pair is linked to regions within the sensor and the helper.

As the integrated HMA is not required for immune activation of the Pik pair and is the most variable domain between the Pikp-1 and Pikm-1 alleles (Costanzo and Jia, 2010), we hypothesised the Pikm-HMA domain co-evolved with Pikm-2 to supress autoactivation mediated by Pik-2 Asp230Glu polymorphism. To test this, we exchanged the integrated HMA domains between sensor alleles Pikp-1 (pHMA) and Pikm-1 (mHMA), to create Pikp-1^{mHMA} and Pikm-1^{pHMA}. Pikp-1^{mHMA} and Pikm-1^{pHMA} were co-expressed in *N. benthamiana* with either the Pikp-2 or Pikm-2 helper and challenged with AVR-PikD or mCherry to test for effector activation and autoimmunity, respectively (**Figure 2 A, Figure S1 A – Appendix 1 B**). Expression of the Pikm-1^{pHMA} with Pikm-2 resulted in effector-independent cell death; however, this sensor was not autoactive in the presence of Pikp-2 and was able to respond to AVR-PikD. By contrast, Pikp-1^{mHMA} was not autoactive when co-expressed with either the Pikp-2 or Pikm-2 helpers and cooperated with either helper to respond to AVR-PikD. These data demonstrate the integrated domain of the Pik-1 sensor contributes to the compatibility between the Pik sensor and helper NLRs.

To gain a better understanding of which features of the HMA domain are involved in sensor/helper compatibility, we generated chimeras by introducing secondary structures from the Pikp-1 HMA into the Pikm-1 HMA and tested for autoactivation in the presence of Pikm-2. The Pik HMA maintains a four-strand β-sandwich fold (β1 – β4) flanked by two helices (α1 and α2) (De la Concepcion et al., 2018). For this experiment we generated six chimeric sensors: Pikm-$1^{\beta1}$, Pikm-$1^{\alpha1}$, Pikm-$1^{\beta2}$, Pikm-$1^{\beta3}$, Pikm-$1^{\alpha2}$, and Pikm-$1^{\beta4}$, and these were co-expressed with Pikm-2 and AVR-PikD or mCherry in *N. benthamiana* (**Figure 2 B, Figure S1 B – Appendix 1 C**). Of the six mutants, only Pikm-$1^{\beta1}$, Pikm-$1^{\alpha2}$, and Pikm-$1^{\beta4}$

resulted in effector-independent cell death. However, not all the residues of the β1 and β4 strands make significant contributions to the AVR-Pik binding interface of the HMA (**Figure 2 C, Figure S2, Figure S3 – Appendix 1 D-F**), implying that some residues not directly involved in the binding to the effector can have a regulatory role in NLR activation. Furthermore, we note co-expression of Pikp-2 with the the Pikm-1$^{\beta4}$ prevented autoactivity caused by co-expression of this chimera with Pikm-2, however we observed a the Pikm-1$^{\beta4}$ to have a reduced response to AVR-PikD when paired with Pikp-2 (Figure 2 B, Figure S1 B – Appendix 1 C). This result may be due to changes to the important interactions between the residues of the β4 strand with the effector, which are known to be more extensive in Pikm-1 than in Pikp-1 (De la Concepcion et al., 2018), or potentially due to the reduced sensitivity of Pikp-2 as a helper (De la Concepcion et al., 2021).

Following the observation that the β1, *α*2, and β4 HMA secondary structures may be involved in helper incompatibility, we created single point mutations of the polymorphic residues between Pikp and Pikm HMA domains in these secondary structures (**Figure S2, Figure S3 – Appendix 1 D-F**) to assess their individual contributions to sensor/helper compatibility. We generated three sets of single mutants in Pikm-1: the β1 mutants Pikm-1^{I184K}, Pikm-1^{M185T}, Pikm-1$^{\Delta G186}$, Pikm-1^{E188L}, Pikm-^{1M189K,} Pikm-1^{F194I}, Pikm-1^{I196V} and Pikm-1^{P197A}; the *α*2 mutants Pikm-1^{S239P}, Pikm-1^{N241K} and Pikm-1^{V243I}; and the β4 mutants Pikm-1^{P252D}, Pikm-1^{M254E}, Pikm-1^{F255L}, Pikm-1^{E257Q}, Pikm-1^{V261A}, Pikm-1^{K262N} and Pikm-1^{E263K}.

These mutants were then co-expressed in *N. benthamiana* with Pikm-2 to test their effect on receptor compatibility. We observed few of the single Pikm-1 mutants to influence compatibility with Pikm-2 in contrast to our observations with the *α*2, β1, and β4 chimeras, which points towards a certain threshold for change in the HMA being tolerated by the

system (**Figure S2, Figure S3 – Appendix 1 D-F**). Notable exceptions to this were the deletion of Gly186 in β1 and the Pro252Asp substitution in β4, which resulted in strong autoactivity in the presence of Pikm-2. Why these two mutations result in such strong autoactivity is unclear, but could be related to both causing large-scale structural changes, as the removal of a residue (ΔG186) or mutation of a proline (Pro252) could impact secondary structure formation and affect the ability of the mHMA to prevent autoactivity in the presence of Pikm-2.

Taken together, these data demonstrate that Pik-1 integrated domain contributes to compatibility with Pik-2 helper NLR and not only to effector binding, as the HMA domain is not required for cell death signalling but has evolved to accommodate for changes in Pik-2 that would otherwise result in constitutive activation.

Integration of the RGA5 HMA domain into Pik-1 is facilitated by allelic mismatching.

Our results also suggest Pikp-2 may be more accommodating of changes in the Pik-1 sensor than Pikm-2, even tolerating the complete substitution of the integrated HMA by an unrelated domain without inducing autoactivity (**Figure 1 – Appendix 1A**). We hypothesised the ability of Pikp-2 to accommodate changes in the integrated domain would allow for integration of an HMA domain that would normally result in autoactivity. To test this, we made a chimera of Pikm-1 carrying the HMA domain from the rice NLR RGA5. Using multiple sequence alignment and structural visualisation in ChimeraX (Pettersen et al., 2021), we defined residues 997 – 1071 from the RGA5 HMA to be the identical boundaries of the Pikm-1 HMA domain. It was important to make sure the size of the HMA incorporated into the Pikm-1 chassis was identical to the Pikm-1 HMA due to our previous

289 observation that removal of a single residue from the HMA (ΔG186) resulted in strong
290 autoactivity.

291 Co-expression of the Pikm-1^{RGA5} chimera with Pikm-2 in *N. benthamiana* resulted in a strong
292 effector-independent cell death response. However, no cell death was observed upon co-
293 expression of Pikm-1^{RGA5} with Pikp-2 (**Figure 3 – Appendix 1 G**). Therefore, the Pikp-2
294 helper allows the integration of the RGA5 HMA into Pikm-1. To test whether the Pikm-1^{RGA5}
295 chimera is a functional receptor, the Pikm-1^{RGA5}/Pikp-2 combination was co-expressed with
296 AVR-Pia. Co-expression of Pikm-1^{RGA5}, Pikp-2 and AVR-Pia in *N. benthamiana* resulted in
297 weak cell death, significantly weaker than the cell death elicited by RGA4/RGA5 in
298 response to AVR-Pia (**Figure 3 – Appendix 1 G**), but comparable to the cross-reactivity of
299 Pikp-1/Pikp-2 with AVR-Pia previously observed in *N. benthamiana* (Varden et al., 2019),
300 indicating a level of cell death equivalent to a known interaction which does not translate
301 into full resistance to *M. oryzae* carrying AVR-Pia in rice plants. Furthermore, we sought
302 determine whether the RGA5 HMA integrated into Pikm-1 could complement the function
303 of the Pikm-1 HMA and respond to AVR-PikD (**Figure S4 – Appendix 1 H).** Co-expression
304 of Pikm-1^{RGA5}/Pikp-2 with AVR-PikD did not trigger a cell death response in *N.*
305 *benthamiana*, demonstrating the RGA5 HMA cannot substitute the Pikm-1 HMA as an AVR-
306 Pik recognition module when integrated into Pikm-1.

307 These data demonstrate the Pikp-2 helper can be used to facilitate the integration of new
308 domains into the Pikm-1 sensor that would otherwise result in autoactivity/incompatibility
309 when paired with Pikm-2.

The RGA5 HMA domain can be engineered to recognise AVR-Pik from within the Pik-1 chassis.

To test whether the RGA5 HMA can act as an effector recognition module in the Pikm-1 receptor, we engineered AVR-Pik recognition in the RGA5 HMA. Using a host target of AVR-Pik, OsHIPP19 (*Oryza sativa* heavy metal-associated isoprenylated plant protein 19) Maidment et al., 2021) as a structural template for AVR-Pik binding we generated an RGA5 variant, termed the AVR-Pik binding (APB) mutant (**Figure S5**). The APB mutant contains the point mutations Glu1033Asp, Val1039Gln, Met1065Gln, Leu1068Glu, Glu1070Lys, and Lys1071Glu that localise to a potential AVR-Pik binding interface of the RGA5 HMA. Next, we generated a Pikm-1 chimera containing the RGA5-APB mutant HMA (Pikm-1^{APB}) and co-expressed it with Pikp-2 and the AVR-Pik variants AVR-PikD, AVR-PikC and AVR-PikF in *N. benthamiana*. The Pikm-1^{APB} chimera was able to trigger cell death in response to AVR-PikD, AVR-PikC and AVR-F (**Figure 4 A, B – Appendix 1 I**). We also tested whether Pikm-1^{APB} could recognise AVR-Pia. However, as for the Pikm-1^{RGA5} chimera, we only observed a weak cell death response **(Figure 4 A, B – Appendix 1 I)**.

To observe whether cell death corresponds with effector binding in planta, we performed co-immunoprecipitation (co-IP) assays with FLAG-tagged Pikm-1^{APB} and 4xMYC tagged AVR-PikD, AVR-PikC, AVR-PikF, AVR-Pia, and PWL2 (Pathogenicity toward Weeping Lovegrass 2) as negative control. We observed bands corresponding to AVR-PikD, AVR-PikC and AVR-PikF in Pikm-1^{APB} samples after FLAG pulldown, whereas only AVR-PikD was pulled down by wildtype Pikm-1 (**Figure 4 C**). Corresponding with the weak response in cell death assays, we were unable to observe association between Pikm-1^{APB} and AVR-Pia.

Taken together, these data demonstrate the RGA5 HMA domain can be engineered to respond to AVR-Pik in planta in the context of the Pikm-1 receptor. However, incorporation of the RGA5 HMA in the Pikm-1 chassis is not sufficient for robust recognition of AVR-Pia.

The affinity of HMA domains for effectors underpins recognition phenotypes in Pik-1 chimeras.

We hypothesized a lower affinity of the APB HMA for AVR-Pia compared to AVR-Pik is responsible for the differences in cell death phenotypes. The interaction between AVR-Pia/RGA5-HMA is known to be much weaker when compared with AVR-Pik/Pik-HMA (De la Concepcion et al., 2018; Guo et al., 2018; Ortiz et al., 2017). To investigate this hypothesis, we performed surface plasmon resonance (SPR) to determine affinities of the RGA5, Pikm-1 and APB HMA domains for different MAX effectors.

We purified AVR-PikD, AVR-PikC, AVR-PikF, AVR-Pia and the non-MAX effector AVR-Pii as previously described (De la Concepcion et al., 2022, 2018) (See materials and methods) and performed multicycle kinetics by flowing the effectors over a Biacore CM5 chip presenting amine-coupled RGA5, APB and Pikm-1 HMA domains (**Figure S6, Table S1**). As in previous reports, we observed strong binding of AVR-PikD to the Pikm-1 HMA (equilibrium dissociation constant (K_D) = ~10 nM) (De la Concepcion et al., 2018) and very low binding to RGA5 HMA (Cesari et al., 2022; Zhang et al., 2022) (**Figure 4 D, Figure S6**); neither the Pikm-1 HMA or RGA5 demonstrated any strong binding to AVR-PikC or AVR-PikF, as characterised by their rapid dissociation from the HMA (**Figure S6 A, Table S1**).

Due to the weak binding of AVR-Pia to the HMAs relative to the Pikm-1/AVR-PikD interaction, higher concentrations (up to 50 μM) of AVR-Pia were flowed over the chip, which allowed us to measure the affinity of AVR-Pia for the RGA5 and APB HMAs at 26.8

and 32.9 μM, respectively (**Figure S6).** These values are in agreement with previous studies that have reported micromolar affinities between the RGA5 HMA and AVR1-CO39 and AVR-Pia effectors using isothermal titration calorimetry (ITC) or microscale thermophoresis (MST) (Guo et al., 2018; Liu et al., 2021; Ortiz et al., 2017; Zhang et al., 2022). Interestingly, the affinity of the interaction between RGA5 HMA and AVR-Pia is similar to the affinities observed for the interaction between RGA5 HMA and AVR-PikD, or Pikm-1 HMA and AVR-PikC/AVR-PikF, which do not to result in resistance in planta. A key similarity between these weaker HMA/effector interactions is the rapid dissociation rate of the effector from the HMA, indicative that the RGA5 HMA alone can facilitate, but not maintain, binding of the effector in vitro. This observation is particularly evident when compared to the binding of Pikm-1 to AVR-PikD in which the dissociation rate is considerably slower (**Figure S6**).

We observed high binding affinity of AVR-PikD, AVR-PikC and AVR-PikF for the APB mutant (**Figure 4 D**). As the effector does not dissociate appreciably from the HMA over the time of the experiment, we were unable to accurately calculate binding using multicycle kinetics (**Figure S7**). Therefore, to quantify the affinity between the APB and AVR-Pik effectors, we used single-cycle kinetics with a long dissociation phase, which allowed us to calculate a K_D of 0.31 nM, 2.95 nM, and 16.50 nM for AVR-PikD, AVR-PikC, and AVR-PikF respectively (**Figure 4 D, Table S1**).

The engineered APB mutant can bind AVR-Pik effectors with nanomolar affinity, and this strong binding corresponds with the effector association and cell death response observed for Pikm-1^{APB} in planta. By contrast, AVR-Pia rapidly dissociates from all HMA domains, and this is corresponds with weak/no response with Pikm-1^{APB} and Pikm-1^{RGA5} chimeras in

planta. Taken together, these data suggest binding affinity to the HMA domain is key to recognition in the Pik system, with high affinity interfaces being essential for initiating a cell death response.

The structural basis for interaction between the RGA5-APB HMA mutant and AVR-Pik.

The Pikm-1 HMA and RGA5 HMA domains are essential for recognition of MAX effectors in their respective NLRs, however they have spatially distinct effector binding interfaces (De la Concepcion et al., 2018; Guo et al., 2018; Ortiz et al., 2017).

As the effector recognition interfaces of RGA5 and Pikm-1 HMA domains are different, we determined a crystal structure of the complex between the APB mutant and AVR-PikF, to validate our structural modelling of the RGA5 HMA and confirm we had engineered an AVR-Pik/Pik-HMA-like interface into RGA5 HMA. Using analytical gel filtration, we observed a peak shift after incubating purified AVR-PikF and APB proteins, indicative of stable complex formation (**Figure 5 A**). Following this, we used a co-expression approach to purify an APB/AVR-PikF complex, which was used to obtain crystals via sparse matrix screening (**Figure S8**). X-ray diffraction data were collected at the Diamond Light Source, Oxford, resulting in a 1.3Å dataset (**Table S2**) **(See details of crystallization and structure solution in materials and methods)**. The APB/AVR-PikF complex shares the same interface as Pikm-1 HMA/AVR-PikD and OsHIPP19/AVR-PikF complexes. Structural alignment of these complexes results in an R.M.S.D. of 0.51 Å and 0.39 Å, respectively (**Figure 5 B, D; Figure S9**). As predicted, each of the six mutations in the RGA5 HMA generated to facilitate AVR-Pik binding are located at the effector interface (**Figure 5 B; Figure S10**). These mutations are sufficient to generate an AVR-Pik binding interface in the RGA5 HMA distinct from that observed for AVR-Pia/AVR1-CO39 (**Figure 5 C**).

Allelic mismatching can alleviate autoactivity cause by the integration of nanobody domains.

Kourelis *et al*. (2023) demonstrated that "Pikobodies", which are defined as Pik-1–nanobody fusions combined with Pik-2, can confer recognition of either eGFP or mCherry upon integration of VHH nanobodies with affinity for these fluorescent proteins. However, some of the nanobodies incorporated into Pikm-1 resulted in constitutive cell death when paired with Pikm-2 (Kourelis et al., 2023). To test whether allelic mismatching could be used to alleviate autoactivity caused by nanobody integration, we performed cell death assays in *N. benthamiana* using five different nanobody integrations, two of which respond to eGFP (Pikm-1^{LaG24} and Pikm-1^{Enhancer}) and three that respond to mCherry (Pikm-1^{LaM2}, Pikm-1^{LaM3} and Pikm-1^{LaM6}) (**Figure 6**; **Figure S11 – Appendix 1 J**) (Kourelis et al., 2023; Fridy et al., 2014, Rothbauer et al., 2006). The Pikm-1–nanobody fusion were co-expressed with Pikm-2 or Pikp-2 in the presence of eGFP or mCherry and assessed for cell death 5 dpi. Of the five nanobody integrations, four were demonstrated to be autoactive in the presence of Pikm-2 (Pikm-1^{LaG24}, Pikm-1^{LaM2}, Pikm-1^{LaM3} and Pikm-1^{LaM6}). While Pikm-1^{LaM3} remained autoactive, the autoactivity of Pikm-1^{LaG24}, Pikm-1^{LaM2} and Pikm-1^{LaM6} could be mitigated by co-expression with Pikp-2, while still retaining recognition of their cognate fluorescent protein, although in the case of Pikm-1^{LaM2} cell death signalling was significantly reduced (**Figure 6**; **Figure S11 – Appendix 1 J**).

Discussion

Constitutive immune activation by the combination of incompatible NLRs through breeding or genetic engineering (hybrid necrosis) presents a bottleneck in plant breeding and evolution (Calvo-Baltanás et al., 2021; Chae et al., 2014; Ordon et al., 2021; Tran et al., 2017). Likewise, autoactivity due to engineering presents a bottleneck to strategies for NLR-mediated pathogen resistance (Kourelis et al., 2023; Maidment et al., 2021; Tamborski et al., 2023). The work presented here highlights the importance of factors outside of enhancing effector binding, such as considering the context of NLRs that act in pairs or networks, for the generation of new recognition specificities and NLR combinations without penalties imposed by constitutive immune activation.

The helper allele Pikp-2 can accommodate for changes in the integrated domain of Pik-1 without triggering effector-independent cell death.

We previously reported on the incompatibility of the Pikp and Pikm alleles (De la Concepcion et al., 2021b), highlighting the functional diversification of the Pik receptor pair and linking the specialisation of the Pik-2 receptor for its cognate sensor to an Asp230Glu polymorphism in the NB domain. How a single amino acid polymorphism with similar chemical properties triggers such a strong phenotype remains obscure. We previously speculated that the extra carbon atom in the side chain of the Glu230 compared with Asp would be enough to create a steric clash or change in conformation that mimics the active state (De la Concepcion et al., 2021), however high-resolution structures of the Pik-2 activated complex would be required to test this hypothesis. In this study, we further demonstrated the role of the integrated HMA domain in compatibility of the Pik-1 sensor with the Pik-2 helper. When we introduced the HMA domain from Pikp-1 into Pikm-1 we observed autoactivity with Pikm-2 but not Pikp-2. Pikp-2^{D230E} and Pikm-2^{E230D} mutants,

444 which flip the specialisation of each helper, swapped the compatibility of Pik-2 for Pik-1
445 mutants/chimeras.

446 Studies involving the swap of the Pikp integrated HMA for a non-co-evolved ancestral
447 version (Białas et al., 2021) or the equivalent HMA domain of OsHIPP19 (Maidment et al.,
448 2022) also showed that this caused autoimmunity, which was removed by mutation of the
449 HMA outside of the effector binding interface, further supporting a mechanism for co-
450 adaptation of the integrated HMA domain with other domains in the sensor Pik-1 and the
451 helper Pik-2. This co-adaptation may have led to different sensitivity thresholds of the
452 helpers for the sensors, resulting in differences in the requirements for activation between
453 Pikp-2 and Pikm-2. As such, we observe Pikp-2 to be more permissive of changes in the Pik-
454 1 compared to Pikm-2.

455 Specific Pik pair combinations are more tolerant to changes in the integrated domain,
456 facilitating engineering of expanded recognition that would otherwise result in constitutive
457 cell death. By considering the context of the engineered receptor domain within the NLR
458 pair, we present an alternative approach to circumventing autoactive immune responses
459 that can limit the potential of NLR engineering for novel disease resistance.

460 **Allelic mismatching provides avenues for engineering disease resistance.**

461 The mismatching strategy reported here opens exciting avenues for the incorporation of new
462 effector recognition motifs into the Pik system, and perhaps other paired NLR systems.
463 Combining the Pikm-1 sensor with the Pikp-2 helper yielded a compatible receptor pair with
464 greater ability to accept HMA modifications than the natural pairing of the Pikm-1/Pikm-2
465 alleles. Mismatching of the Pik sensor/helper alleles allowed incorporation of the RGA5
466 HMA into the Pikm-1 backbone, without autoactivity. Notably, this strategy appears to be

467 useful in areas such as the incorporation of VHH-nanobody fusions into Pikm-1 to allow for
468 tailor-made NLRs deemed 'Pikobodies' (Kourelis et al., 2023), which are often autoactive in
469 the presence of Pikm-2. Indeed, we demonstrate several Pikm-1–VHH-nanobody chimeras
470 triggered constitutive cell death responses, indicative of autoactivity, and this autoactivity
471 can be mitigate through co-expression of the Pikp-2 helper. Mismatching of the Pik alleles in
472 conjunction with nanobody integration is a powerful combination that could allow for a
473 greater number of successful integrations, streamlining this engineering strategy.

474 Recently, there have been several reports of engineering expanded effector recognition in
475 integrated HMA domain containing NLRs (Cesari et al., 2022; De la Concepcion et al., 2019;
476 Liu et al., 2021; Maidment et al., 2022; Zhang et al., 2022). In the RGA5/RGA4 system,
477 recognition of AVR-Pib and AVR-PikD has been engineered into the RGA5 HMA domain,
478 however this results in compromised AVR-Pia recognition (Cesari et al., 2022; Liu et al.,
479 2021; Zhang et al., 2022). Furthermore, implementation of model-driven engineering of
480 RGA5 into crop systems is challenging and has had variable success, with RGA5 mutants
481 that exhibit expanded recognition in a *N. benthamiana* model not always translating to
482 disease resistance in transgenic rice lines (Cesari et al., 2022; Zhang et al., 2022). In parallel,
483 engineering of the Pikp-1 HMA to respond to previously unrecognised AVR-Pik variants
484 has been shown in *N. benthamiana* assays and transgenic rice lines (Maidment et al., 2022).

485 Interestingly, full replacement of the integrated HMA for the HMA domain of OsHIPP19
486 caused autoimmunity, which was removed by mutation of the HMA. However, this is not
487 always possible as the approach benefitted from knowledge of the NLR-ID/effector
488 complex (Białas et al., 2021; De la Concepcion et al., 2019; Maidment et al., 2022). Whether
489 engineering facilitated by allelic mismatching of the Pik pair can provide resistance in

transgenic rice lines is yet to be tested and is an important next step to demonstrate the use of this approach for translating recognition in plant models to resistance in crops.

The Pik system relies on high affinity effector binding to activate defence responses in planta.

We demonstrate the RGA5 HMA domain can be integrated into the Pikm-1 backbone and engineered to recognise AVR-Pik, including variants not recognised by wildtype Pikm-1. As shown by our biophysical and structural analysis, the six mutations introduced in the APB mutant of RGA5 HMA domain, based on the host target OsHIPP19, recapitulate a functional AVR-Pik binding recognition interface. These data highlight the power of host target-guided design of NLR-ID baits for engineering recognition.

While low levels of cell death were observed, neither Pikm-1^{RGA5} nor Pikm-1^{APB} responded to AVR-Pia at a level comparable with RGA5/RGA4. Indeed, the cell death observed is better compared to the cell death caused the Pikp pair when co-expressed with AVR-Pia, which has been described as cross-reactivity in *N. benthamiana*, as Pikp is unable to provide full resistance to *M. oryzae* strains carrying AVR-Pia (Varden et al., 2019). It is possible the AVR-Pia/AVR1-CO39 interface is occluded in the Pikm-1^{RGA5} chimera, and co-IP with the APB mutant did not show an association in planta. However, we speculate that the lack of AVR-Pia recognition *N. benthamiana* is likely due to a naturally lower affinity of the effector for the HMA domain opposed to occlusion of the interaction interface, as we were able to observe some weak cell death when Pikm-1^{RGA5} or Pikm-1^{APB} co-expressed with Pikp-2 was challenged with AVR-Pia. Indeed, substitution of VHH nanobodies that share no homology to the effector recognition interfaces of HMA domains are able to act as sensory domains for the Pikm-1 sensor, making the hypothesis that reduced response to AVR-Pia by the Pikm-

513 1^{RGA5} and Pikm-1^{APB} receptor is due to an occluded RGA5/AVR-Pia interface less likely. In
514 support of this, previous studies have benchmarked the affinity of AVR-Pia/AVR1-CO39 for
515 the RGA5 HMA domain in the micromolar range (Guo et al., 2018; Ortiz et al., 2017), while
516 AVR-Pik effectors bind their cognate integrated HMA domains with nanomolar affinity (for
517 interactions that result in cell death responses). These previous observations were
518 corroborated by the biophysical analyses performed in this study (**Figure S6 A, Table S1**),
519 which also measure the affinities of RGA5 and the APB HMA domains for AVR-Pia in the
520 micromolar range, compared to the nanomolar affinities of the APB HMA and Pikm-1 HMA
521 domains for AVR-Pik effectors.

522 It remains unclear why the binding affinities of the Pik HMA and RGA5 HMA domains for
523 their cognate effectors differ so significantly. However, the RGA5 post-LRR region, which
524 contains the HMA domain, also contains several other small uncharacterised domains
525 (**Figure S12**), which may contribute to effector binding. Indeed, AVR-Pia is known to
526 associate with regions of the RGA5 receptor outside of the HMA domain (Ortiz et al., 2017).
527 However, RGA5 receptors where the HMA domain has been deleted are unable to respond
528 to AVR-Pia in cell death assays (Cesari et al., 2013). Furthermore, recent studies engineering
529 AVR-Pib and AVR-Pik recognition in RGA5, respectively, showed mutations outside of the
530 HMA influenced effector recognition in planta (Liu et al., 2021; Zhang et al., 2022).
531 Collectively, available data suggest that RGA5-mediated effector recognition requires the
532 HMA domain, but alone it is not sufficient for effector recognition, and works together with
533 other regions at the RGA5 C-terminus. Inclusion of these additional regions from RGA5 into
534 the Pik receptor backbone alongside the RGA5 HMA domain could support AVR-Pia
535 recognition, but equally so, may affect Pik sensor/helper compatibility. Certainly, the

additional complexity of the RGA4/RGA5 system makes engineering this receptor pair more challenging compared to the Pik NLRs.

Modification of plant NLRs has proven challenging due to the lack of understanding of the context of NLRs as part of complex systems. In this study, we facilitate NLR-mediated resistance engineering through exploiting the allelic diversity in the Pik NLR pair to allow for generation of receptors with expanded recognition specificities that would otherwise result in constitutive cell death. Our structural, biophysical and in planta analyses demonstrate the Pik system requires a high affinity effector binding interface to allow for binding to translate to defence, and as a single domain, the RGA5 HMA domain appears to lack the affinity for AVR-Pia to facilitate a robust Pik chassis-mediated cell death response. However, our engineering of RGA5 HMA to recognise AVR-Pik from within the Pikm-1 chassis highlights the strengths of this system for engineering; only a single high-affinity interface needs to be present to mediate effector recognition, making the Pik system a simple but efficient means for generating bespoke NLR resistance. This work lays the foundation for the incorporation of new effector recognition motifs into the Pik system and is a key advance towards the development of designer NLRs that can be tailored to specific secreted pathogen signatures.

Materials and Methods

Plant materials and growth conditions

Nicotiana benthamiana plants were grown in a controlled environment room at 22°C constant temperature and 80% relative humidity, with a 16 hour photoperiod with lighting provided by a combination of two Philips Master TL-D 58W/840 and Sylvania GRO-LUX F58W/GRO-T8 fluoresent tubes.

Gene cloning – in planta expression

For expression in planta, full length *Pikp-1* and *Pikm-1*, and relevant mutants, were cloned with a 6xHIS/3xFLAG tag into the pICH47742 plasmid, full length *Pikp-2* and *Pikm-2* were cloned by GoldenGate cloning via *Bsa1* into pICH47751 with a C-terminal 6xHA tag and *Pikp-2*^{D230E} and *Pikm-2*^{E230D} mutants were generated by site-directed mutagenesis as previously described (De la Concepcion et al., 2021b, 2018).

To generate the Pikm-1 DOM2 acceptor, the *Pikm-1* sequence was domesticated of *BsaI* and *BbsI* restriction sites to allow compatibility with our Golden Gate cloning system and cloned into the Level 0 CDS(ns) pICSL01005 acceptor. Once domesticated, the position of the *Pikm-1* HMA domain was substituted with pre-domesticated iGEM amilCP negative selection reporter cassettes internally flanked by outward pointing *Esp3I* sites to produce CAGA (5′) and GATG (3′) cloning overhangs. *Esp3I* was used to incorporate an iGEM RFP negative selection reporter cassette, internally flanked by outward pointing *BbsI* sites presenting CAGA (5′) and GATG (3′) cloning overhangs, allowing cloning of new domains via *BbsI* into the Pikm-1 DOM2 acceptor in the analogous position to where the HMA domain was located.

The *RGA5* HMA and APB mutant were cloned into the Pikm-1 DOM2 acceptor via Golden Gate cloning with *BbsI* to assemble a full length *Pikm-1* receptor chimera. Full length *Pikm-1*^{RGA5} and *Pikm-1*^{APB} were subsequently cloned into pICH47742 via *BsaI*, with a C-terminal 6xHIS/3xFLAG tag.

RGA5/RGA4 were assembled into the binary Agrobacterium (*Agrobacterium tumefaciens*) expression vector pICSL4723 (Engler et al., 2014) via *BbsI*. *RGA4* was tagged with a C-terminal 6xHA tag and *RGA5* was left untagged to prevent effects on receptor function. Expression of *RGA4* and *RGA5* was driven by the Arabidopsis (*Arabidopsis thaliana*) actin and 2x35S promoters, respectively. For cell death assays, AVR-Pia was cloned untagged into pJK268c with P19 via *Bbs1*, with expression driven by a 2x35S promoter. For co-IP assays, an N-terminally 4xMYC tagged AVR-Pia was cloned into pICH47752 via *Bsa1*.

AVR-Pik effector variants used in this study were described previously (De la Concepcion et al., 2018). *PWL2* was cloned into pICH47751 under a Ubi10 promoter and 35S terminator and C-terminal 4xMYC tag via Golden Gate cloning.

Pikobody constructs for co-expression of *Pikm-2* with the *Pikm-1* nanobody fusions, either the LaG24, GFP enhancer, LaM2, LAM3, or LAM6 nanobody were described in Kourelis et al., 2023. For mismatching, the above constructs were redesigned to co-express *Pikp-2* rather than *Pikm-2*.

Gene cloning – recombinant expression in *Escherichia coli*

The *RGA5*, *APB* and *Pikm-1* HMA domains as well as the *AVR-Pik* effector variants and *AVR-Pia* effector were cloned into pOPIN-GG vector pPGN-C iva (Bentham et al., 2021) with a cleavable N-terminal 6xHIS-GB1-3C tag via Golden Gate cloning with *BsaI*. *AVR-Pii*

effector domain was cloned with a cleavable N-terminal MBP tag and an uncleavable C-terminal 6xHIS via In-fusion cloning into pOPINE (Berrow et al., 2007). For co-expression with the *APB* HMA for crystallography studies, *AVR-PikF* was cloned into pPGC-K (Bentham et al., 2021) without a tag via Golden Gate cloning with *BsaI*.

In planta co-immunoprecipitation (co-IP)

Transient gene expression in planta was performed by infiltrating 4 week old *Nicotiana benthamiana* plants with *A. tumefaciens* strain GV3101 (C58 (rifR) Ti pMP90 (pTiC58DT-DNA) (gentR) Nopaline (pSoup-tetR). *A. tumefaciens* carrying NLRs and effectors were infiltrated at OD_{600} 0.4 and 0.6, respectively, in agroinfiltration medium (10 mM $MgCl_2$, 10 mM 2-(N-morpholine)-ethanesulfonic acid (MES), pH 5.6) with the addition of 150 µM acetosyringone.

Leaf tissue was collected 3 days post infiltrations (dpi) and frozen in liquid nitrogen before processing. Samples were ground to a fine powder in liquid nitrogen using a mortar and pestle before being mixed with two times weight/volume ice-cold Co-IP extraction buffer (25 mM Tris pH 7.5, 150 mM NaCl, 1 mM EDTA, 10 % v/v glycerol, 2 % w/v PVPP, 10 mM DTT, 1 x cOmplete protease inhibitor tablet per 50 mL (Roche), 0.1 % Tween20). Samples were centrifuged at 4200 *g* at 4°C for 20 min, and supernatant was passed through a 0.45 µm Ministart syringe filter. SDS-PAGE/immunoblot analysis was used to identify proteins in the sample with use of anti-FLAG M2 antibody (Sigma) and anti-MYC antibody (Santa Cruz Biotechnology) for NLRs and effectors, respectively.

For immunoprecipitation, 2 mL of filtered plant extract was incubated with 30 µL of M2 anti-FLAG magnetic beads (Sigma) in a rotary mixer for 3 hrs at 4°C. The FLAG beads were separated from the supernatant with use of a magnetic rack to allow for the removal of the supernatant. The beads were then washed with 1 mL of IP buffer (25 mM Tris pH 7.5, 150

mM NaCl, 1 mM EDTA, 10 % glycerol, 0.1 % Tween20). The FLAG beads were washed three times using this method. After washing, 30 µL of LDS Runblue sample buffer was added to the FLAG beads and incubated for 10 min at 70°C. The beads were then applied to a magnetic rack and the supernatant was loaded to SDS-PAGE gels and subsequently used for immunoblot blot analysis. PVDF membranes were probed with anti-FLAG M2 and anti-MYC antibodies to detect NLRs and effectors, respectively.

N. benthamiana cell death assays and cell death scoring

Cell death assays and scoring were performed as described previously (De la Concepcion et al., 2021). In brief, *N. benthamiana* tissue was infiltrated with *A. tumefaciens* GV3101 (C58 [rifR] Ti pMP90 [pTiC58DT-DNA] [gentR] Nopaline [pSoup-tetR]) carrying NLRs and effectors at OD_{600} 0.4 and 0.6 respectively, and P19 at OD_{600} 0.1. Leaves were imaged 5 dpi from the abaxial side for UV fluorescence images. Photos were taken using a Nikon D4 camera with a 60 mm macro lens, ISO set 1600 and exposure ~10 secs at F14. The filter was a Kodak Wratten No.8 and white balance was set to 6250 degrees Kelvin. Blak-Ray longwave (365 nm) B-100AP spot light lamps were moved around the subject during the exposure to give an even illumination. Images shown are representative of three independent experiments with a minimum internal technical repeats, a minimum of 45 data points across three repeats were collected per sample across 30 plants. The cell death scoring was performed using the cell death index previously presented in Maqbool et al., 2015. Dot plots were generated using R 4.0.5 (https://www.r-project.org) with the packages ggplot2 (Wickham, 2016). The size of the centre dot at each cell death value is directly proportional to the number of replicates in the sample with that score. All individual data points are represented as dots. Statistical analysis was performed using estimation graphics (Ho et al.,

2019) with the besthr R package (De la Concepcion et al., 2021b; MacLean, 2019) and can be found in Appendix 1.

Protein expression and purification from *E. coli*

Expression vectors containing the 6xHIS-GB1-tagged effectors and HMA domains were transformed into *E. coli* SHuffle cells. Using an overnight culture for inoculum, 8 L of SHuffle cells were grown in autoinduction media (AIM) at 30°C to an OD_{600} of 0.6 – 0.8 before the temperature was reduced to 18°C for overnight induction (Studier, 2005). Cells were pelleted by centrifugation at 5000 *g* for 10 mins and resuspended in lysis buffer (50 mM HEPES pH 8.0, 500 mM NaCl, 30 mM imidazole, 50 mM glycine and 5 % v/v glycerol). Cell lysate was clarified by centrifugation at 45000 *g* for 20 mins following disruption of the resuspended pellet by sonication. Proteins were purified from clarified lysate via Ni^{2+} immobilised metal chromatography (IMAC) coupled with size-exclusion chromatography (SEC). The 6xHIS-GB1 tag was removed via overnight cleavage with 3C protease at 4°C before a final round of SEC using a buffer of 10 mM HEPES pH 8, 150 mM NaCl. Proteins were flash frozen in liquid nitrogen before storage at -80°C.

For co-expression of the APB/AVR-PikF complex, *E. coli* SHuffle cells were co-transformed with 6xHIS-GB1-tagged APB HMA and untagged AVR-PikF and plated on dual resistance carbenicillin and kanamycin selection. Expression and purification of the complex was then performed as described above, using dual selection for growth in large scale cultures.

Crystallization, x-ray data collection, structure solution and refinement.

The APB/AVR-PikF complex was concentrated to 10 mg/mL in SEC buffer (10 mM. HEPES pH 8.0, 150 mM NaCl) for crystallisation. Sitting drop, vapour diffusion crystallisation trials were set up in 96-well plates using an Oryx Nano robot (Douglas Instruments).

Crystallisation plates were incubated at 20°C. APB/AVR-PikF crystals appeared in the SG1 ™ Screen (Molecular Dimensions) after 10 days in a 0.1 M BIS-TRIS pH 5.5, 25 w/v % PEG 3350 condition. Crystals were harvested and snap frozen in liquid nitrogen prior to shipping.

Crystals of the APB/AVR-PikF complex diffracted to 1.3 Å and x-ray datasets were collected at the Diamond Light Source on the i04 beamline under proposal mx25108. The data were processed using the xia2 pipeline and AIMLESS as implemented in CCP4i2 (Winn et al., 2011). Using the structure of the OsHIPP19/AVR-PikF complex (PDB ID: 7B1I) as a template, the structure of the APB/AVR-PikF complex was solved using molecular replacement with PHASER (McCoy et al., 2007). The final structure was obtained after iterative cycles of refinement using COOT and REFMAC (Emsley and Cowtan, 2004; Murshudov et al., 1997). Structure geometry was validated using the tools in COOT and MOLPROBITY (Chen et al., 2010; Emsley and Cowtan, 2004). Protein interface analyses were performed using QtPISA and ChimeraX (Krissinel and Henrick, 2007; Pettersen et al., 2021). Models are visualised using ChimeraX (Pettersen et al., 2021). X-ray diffraction data can be found in the Protein Data Bank (https://www.ebi.ac.uk/pdbe/) under the accession number 8B2R.

Analytical size-exclusion chromatography

150 µg of purified AVR-PikF was mixed with 150 µg of the RGA5 and APB HMA domains and incubated on ice for 30 mins before separation via SEC using a Superdex S75 10/300 GL size-exclusion column (Cytiva). As a negative control, 150 µg of AVR-PikF was run alone. HMA domains were not run separate from AVR-PikF due to low or no absorbance at A_{280}

resulting in no observable peak in the chromatogram. Chromatograms were visualised using the ggplot2 R library in R 4.0.5 (Wickham, 2016).

Biophysical analysis with surface plasmon resonance.

Surface plasmon resonance was performed using a Biacore 8K (Cytiva). Purified HMA domains were immobilised on a Series S Sensor CM5 Chip (Cytiva) via amine-coupling using 0.4 M 1-ethyl-3-(3-dimethylaminopropyl)-carbodiimide (EDC) and 0.1 M N-hydroxysuccinimide (NHS) to activate the chip surface prior to binding of HMAs at two concentrations on different channels, a high concentration (30 nM, ~2000 response units (RU)) and a low concentration (0.3 nM, ~200 RU) to allow for accurate measurement of affinity and kinetics of strong and weak interactors. 1 M ethanolamine-HCl pH 8.5 was then used to block the CM5 chip after coupling was completed.

Samples were run in HBS-EP+ running buffer (0.1 M HEPES, 1.5 M NaCl, 0.03 M EDTA and 0.5% v/v Tween20) and the chip was regenerated after each cycle with an ionic regeneration buffer (0.46 M KSCN, 1.83 M $MgCl_2$, 0.92 M urea, 1.83 M guanidine-HCl). Effectors were run over the chip at a flow rate of 100 µL/min; contact and dissociation time varied depending on the experiment (see below).

Where possible, we performed multicycle kinetics to assess the affinity and binding kinetics of the effectors for the HMA. For strong interactions (Pikm-1 HMA with AVR-PikD) we used serial dilutions of effectors from 50 nM – 0 nM, and for weak interactions we used serial dilutions of 50 µM – 0 µM (AVR-Pia with RGA5 HMA, APB HMA and Pikm-1 HMA; AVR-PikC with RGA5 HMA and Pikm-1 HMA; AVR-PikF with RGA5 HMA and Pikm-1 HMA), with each concentration being performed in triplicate. Contact time and dissociation times for the experiment were set at 120 s.

For strong interactions we performed single-cycle kinetics due to the extremely slow dissociation rates of the effectors from the HMA domains, which interfered with accurate calculations of kinetic parameters and binding affinity. For single cycle kinetics, increasing concentrations of effector (0 nM – 50 nM) were sequentially flowed over the HMA-bound sensor chip each with a contact time of 120 s before a single dissociation phase of 600 s. Each cycle was performed in triplicate.

SPR sensograms were analysed with the Biacore Insight Evaluation Software (Cytiva) and equilibrium dissociation constants (K_D) values were calculated using a 1:1 binding model from a kinetic fit model. Residual graphs are generated from the subtraction of the experimental data from the fit model (ΔFit – Exp). Sensograms and residual graphs were generated in R 4.0.5 using the ggplot2 R package (Wickham, 2016).

Accession Numbers

Pikp-1 E9KPB5, Pikm-1 B5UBC1, Pikp-2 and Pikm-2 D5L9H7, RGA5 F7J0N2, RGA4 F7J0M4, AVR-Pik (variants D, C, and F) C4B8C2, AVR-Pia B9WZW9, AVR-Pii L7J571, PWL2 A0A3G2LZD8.

Funding Information

This work was supported by UKRI Biotechnology and Biological Sciences Research Council (BBSRC) Norwich Research Park Biosciences Doctoral Training Partnership, (grant BB/M011216/1); the UKRI BBSRC, UK (grants BB/P012574/1, BBS/E/J/000PR9797) the European Research Council (ERC proposal 743165), the ERAMUS+ training programme, the John Innes Foundation and the Gatsby Charitable Foundation.

Acknowledgments

We thank the Diamond Light Source, UK (beamline i04 under proposal 25108) for access to X-ray data collection facilities and Dave Lawson from the JIC Protein Crystallography Platform for expert technical assistance during data collection. We thank Dan McLean for technical advice with the besthr R package. We further thank all members of the BLASTOFF

team at the Sainsbury Laboratory, John Innes Centre and Iwate Biotechnology Research Center. We especially thank Vincent Were for providing PWL2 constructs.

Author Contributions

ARB, JCDlC, JK and MJB designed the research. ARB, JCDlC, JVB, JK, SJ performed the experiments. ARB, JCDlC, CEMS and MJB analyzed the data. SJ, MM, JS, assisted with preliminary experiments. CEMS provided key technical advice. JK, JHRM, RZ and MY contributed key genetic resources. ARB, JCDlC and MJB wrote the manuscript with input from all authors.

Figure Legends

Figure 1. Pik-2 polymorphisms determine Pik-1 HMA domain independent allelic compatibility. A) Schematic diagram highlighting the domain architecture of Pikp-1 and Pikp-1$^{\Delta HMA}$ sensor NLRs (nucleotide-binding leucine-rich repeat receptors) and the polymorphisms between the Pikp-2 and Pikm-2 helper NLRs. **B)** *N. benthamiana* cell death assays of Pikp-1$^{\Delta HMA}$ co-expressed with Pik-2 helpers and mutant variants visualised via ultraviolet light. The HMA (heavy metal-associated) domain of Pikp-1 is not required for effector-independent cell death in *N. benthamiana*; compatibility remains with Pikp-2 but not Pikm-2. Reciprocal D230E and E230D mutations in Pikp-2 and Pikm-2 flip the compatibility of the helper NLRs for Pikp-1$^{\Delta HMA}$. The other polymorphic residues between Pikp-2 and Pikm-2, T434S and M627V, have no effect on helper compatibility. **C)** Cell death scoring for repeats of Pikp-1$^{\Delta HMA}$ co-expressed with Pikp-2, Pikm-2, and mutants in *N. benthamiana* represented as dot plots. The total number of repeats was spots 75 per sample. For each sample, all the data points are represented as dots with a distinct colour for each of the three biological replicates; these dots are jittered around the cell death score for visualisation

796 purposes. The size of the central dot at each cell death value is proportional to the number of
797 replicates of the sample with that score. Quantification and statistical analysis of these
798 results can be found in **Appendix 1 A**. Details of the NLR mutants used in these experiments
799 can be found in **Table S3**.

800 **Figure 2. The HMA domain of Pik-1 is important for compatibility with Pik-2 helpers. A)**
801 Co-expression of Pikp-1 with Pikm-2 triggers effector-independent cell death in *N.*
802 *benthamiana.* Integration of the Pikm-1 HMA into Pikp-1 facilitates Pikp-1 compatibility with
803 Pikm-2, whereas incorporation of the Pikp-1 HMA into Pikm-1 abolishes compatibility with
804 Pikm-2. Quantification and statistical analysis of these results are shown in **Figure S1 A,**
805 **Appendix 1 B. B)** Incompatibility of the Pikp-1 with Pikm-2 in *N. benthamiana* is linked to
806 the α2 helix, β1, and β4 strands of the HMA (heavy metal-associated) domain, with Pikm-1
807 HMA chimeras carrying the Pikp-1 secondary structure elements resulting in effector-
808 independent cell death when co-expressed with Pikm-2. Quantification and statistical
809 analysis of these results can be found in **Figure S1 B, Appendix 1 C. C)** Some regions of the
810 HMA domain that are involved in sensor/helper incompatibility (blue) are shared with the
811 AVR-Pik binding interface (PDB ID: 6FU9). Details of the NLR mutants used in these
812 experiments can be found in **Table S3**.

813 **Figure 3. Autoactivity following integration of the RGA5 HMA domain into Pikm-1 is**
814 **relieved by allelic mismatch with Pikp-2, but only weakly responds to AVR-Pia.** A)
815 Schematic structural alignment of the RGA5 HMA (heavy metal-associated) domain (blue;
816 PDB ID: 5ZNG) with the Pikm-1 HMA domain (yellow; PBD ID: 6FU9) showing the
817 different binding interfaces of these HMAs for the AVR-Pik (vermillion) and AVR1-CO39
818 (pink)/AVR-Pia (not shown) effectors. B) Co-expression of Pikm-1^{RGA5} with Pikp-2

supresses effector independent cell death in the presence of empty vector (EV) control and responds weakly to AVR-Pia. C) Cell death scoring of wildtype (WT) Pikm-1 and Pikm-1^{RGA5} co-expressed with Pikp-2 in *N. benthamiana* represented as dot plots. The total number of repeats was 45 per sample. For each sample, all the data points are represented as dots with a distinct colour for each of the three biological replicates; these dots are jittered around the cell death score for visualisation purposes. The size of the central dot at each cell death value is proportional to the number of replicates of the sample with that score. Statistical analyses of these results are shown in **Appendix 1 G**. Details of the NLR (nucleotide-binding leucine rich repeat receptor) mutants used in these experiments can be found in **Table S3**.

Figure 4. The RGA5 APB mutant binds and recognises AVR-Pik when integrated into Pikm-1. A) Pikm-1^{APB} chimera responds to all variants of AVR-Pik tested and activates cell death when co-expressed with Pikp-2 in *N. benthamiana*, but like Pikm-1^{RGA5}, it only weakly responds to AVR-Pia. **B)** Cell death scoring of Pikm-1^{APB} co-expressed with AVR-Pik variants D, C and F in *N. benthamiana* represented as dot plots. The total number of repeats was 80 per sample. For each sample, all the data points are represented as dots with a distinct colour for each of the three biological replicates; these dots are jittered around the cell death score for visualisation purposes. The size of the central dot at each cell death value is proportional to the number of replicates of the sample with that score. Statistical analyses of these results are shown in **Appendix 1 I C)** Co-immunoprecipitation of Pikm-1^{APB} with different MAX (*Magnaporthe* AVRs and ToxB-like) effectors shows association with AVR-Pik variants, but not AVR-Pia, in planta. Dotted line denotes separate membrane exposures of the same membrane. **D)** Surface plasmon resonance (SPR) sensograms for the interaction of HMA (heavy metal-associated) domains of Pikm-1, RGA5 and RGA5 APB mutant with effectors AVR-PikD, AVR-PikC, AVR-PikF and AVR-Pia. Non-MAX effector AVR-Pii was

added as a negative control. Response units for each labelled protein concentration are shown with the residuals plot beneath (SPR acceptance guides as determined by Biacore software are shown as green and red lines in the residuals plots). Concentration of each protein in the assay is indicated next to their corresponding name. Each experiment was repeated a minimum of 3 times, with similar results.

Figure 5. Six mutations in the RGA5 HMA reconstitutes a high affinity AVR-Pik binding interface akin to that of the Pik-1 HMA. A) Analytical size-exclusion chromatography of AVR-PikF with the RGA5 and APB HMA (heavy metal-associated) proteins. A mixture of AVR-PikF and APB HMA (green) elutes earlier than a mixture of RGA5 and AVR-PikF (blue) or AVR-PikF alone (sky blue), indicative of complex formation between AVR-PikF and the APB HMA. **B)** The crystal structure of AVR-PikF (sky blue) in complex with the RGA5 APB HMA mutant (green) (PDB: 8B2R). Mutations in RGA5, guided by the structure of the OsHIPP19/AVR-PikF complex, are shown forming contacts with AVR-PikF and are labelled. **C)** Superimposition of the crystal structures of the APB/AVR-PikF complex (sky blue / green) with the RGA5/AVR1-CO39 complex (blue / pink) (PDB ID: 5ZNG) showing the swapped effector-binding interface of the APB HMA compared to the RGA5 HMA. **D)** Superimposition of the APB/AVR-PikF complex with the crystal structure of AVR-PikD (vermillion) bound to the Pikm-1 HMA domain (yellow) (PDB ID: 6G10), showing the shared effector binding interface in these complexes.

Figure 6. Allelic mismatching of the Pik helper NLRs can be used to alleviate autoactivity from nanobody integration in Pikm-1. Five pikobodies that either respond to the fluorescent protein eGFP (enhanced green fluorescent protein) (Pikm-1^{LaG24} and Pik-1^{Enhancer} indicated by green text) or mCherry (Pikm-1^{LaM2}, Pikm-1^{LaM3} and Pikm-1^{LaM6}, indicated by

red text) were tested with the Pikm-2 or Pikp-2 helpers to assess the effect of mismatching on cell death responses in *N. benthamiana*. **A, B)** Pikm-1^{LaG24} and Pikm-1^{LaM6} are autoactive in the presence of Pikm-2, however co-expression with the Pikp-2 helper does not result in autoactivity. Both pikobodies retain ability to respond to their respective fluorescent proteins **C)** Pikm-1^{Enhancer} is not autoactive in the presence of both helpers and can respond to eGFP with equal strength. **D)** Co-expression of Pikm-1^{LaM2} with Pikp-2 alleviates autoactivity observed in the presence of Pikm-2, however response to mCherry is substantially reduced. **E)** Mismatching of the helper alleles is unable to prevent autoactivity induced by the Pikm-1^{LaM3} pikobody. Details of the NLR (nucleotide-binding leucine rich repeat receptor) mutants used in these experiments can be found in **Table S3**.

References

Adachi, H., Derevnina, L., Kamoun, S., 2019. NLR singletons, pairs, and networks: evolution, assembly, and regulation of the intracellular immunoreceptor circuitry of plants. Curr Opin Plant Biol 50, 121–131. https://doi.org/10.1016/j.pbi.2019.04.007

Baggs, E., Dagdas, G., Krasileva, K., 2017. NLR diversity, helpers and integrated domains: making sense of the NLR IDentity. Current Opinion in Plant Biology, 38 Biotic interactions 2017 38, 59–67. https://doi.org/10.1016/j.pbi.2017.04.012

Bentham, A.R., De la Concepcion, J.C., Mukhi, N., Zdrzałek, R., Draeger, M., Gorenkin, D., Hughes, R.K., Banfield, M.J., 2020. A molecular roadmap to the plant immune system. JBC 295, 14916–14935. https://doi.org/10.1074/jbc.REV120.010852

Bentham, A.R., Youles, M., Mendel, M.N., Varden, F.A., Concepcion, J.C.D. la, Banfield, M.J., 2021. pOPIN-GG: A resource for modular assembly in protein expression vectors. https://doi.org/10.1101/2021.08.10.455798

Berrow, N.S., Alderton, D., Sainsbury, S., Nettleship, J., Assenberg, R., Rahman, N., Stuart, D.I., Owens, R.J., 2007. A versatile ligation-independent cloning method suitable for high-throughput expression screening applications. Nucleic Acids Res 35, e45. https://doi.org/10.1093/nar/gkm047

Białas, A., Langner, T., Harant, A., Contreras, M.P., Stevenson, C.E., Lawson, D.M., Sklenar, J., Kellner, R., Moscou, M.J., Terauchi, R., Banfield, M.J., Kamoun, S., 2021. Two NLR

immune receptors acquired high-affinity binding to a fungal effector through convergent evolution of their integrated domain. eLife 10, e66961. https://doi.org/10.7554/eLife.66961

Białas, A., Zess, E.K., De la Concepcion, J.C., Franceschetti, M., Pennington, H.G., Yoshida, K., Upson, J.L., Chanclud, E., Wu, C.-H., Langner, T., Maqbool, A., Varden, F.A., Derevnina, L., Belhaj, K., Fujisaki, K., Saitoh, H., Terauchi, R., Banfield, M.J., Kamoun, S., 2018. Lessons in Effector and NLR Biology of Plant-Microbe Systems. MPMI 31, 34–45. https://doi.org/10.1094/MPMI-08-17-0196-FI

Bomblies, K., Lempe, J., Epple, P., Warthmann, N., Lanz, C., Dangl, J.L., Weigel, D., 2007. Autoimmune response as a mechanism for a Dobzhansky-Muller-type incompatibility syndrome in plants. PLoS Biol 5, e236. https://doi.org/10.1371/journal.pbio.0050236

Burdett, H., Kobe, B., Anderson, P.A., 2019. Animal NLRs continue to inform plant NLR structure and function. Archives of Biochemistry and Biophysics, Inflammasomes: Intracellular mediators of immune defence 670, 58–68. https://doi.org/10.1016/j.abb.2019.05.001

Calvo-Baltanás, V., Wang, J., Chae, E., 2021. Hybrid Incompatibility of the Plant Immune System: An Opposite Force to Heterosis Equilibrating Hybrid Performances. Frontiers in Plant Science 11.

Cesari, S., 2018. Multiple strategies for pathogen perception by plant immune receptors. New Phytologist 219, 17–24. https://doi.org/10.1111/nph.14877

Cesari, S., Bernoux, M., Moncuquet, P., Kroj, T., Dodds, P.N., 2014. A novel conserved mechanism for plant NLR protein pairs: the "integrated decoy" hypothesis. Front Plant Sci 5, 606. https://doi.org/10.3389/fpls.2014.00606

Cesari, S., Thilliez, G., Ribot, C., Chalvon, V., Michel, C., Jauneau, A., Rivas, S., Alaux, L., Kanzaki, H., Okuyama, Y., Morel, J.-B., Fournier, E., Tharreau, D., Terauchi, R., Kroj, T., 2013. The Rice Resistance Protein Pair RGA4/RGA5 Recognizes the Magnaporthe oryzae Effectors AVR-Pia and AVR1-CO39 by Direct Binding. The Plant Cell 25, 1463–1481. https://doi.org/10.1105/tpc.112.107201

Cesari, S., Xi, Y., Declerck, N., Chalvon, V., Mammri, L., Pugnière, M., Henriquet, C., de Guillen, K., Chochois, V., Padilla, A., Kroj, T., 2022. New recognition specificity in a plant

homo immune receptor by molecular engineering of its integrated domain. Nat Commun 13, 1524. https://doi.org/10.1038/s41467-022-29196-6

Chae, E., Bomblies, K., Kim, S.-T., Karelina, D., Zaidem, M., Ossowski, S., Martín-Pizarro, C., Laitinen, R.A.E., Rowan, B.A., Tenenboim, H., Lechner, S., Demar, M., Habring-Müller, A., Lanz, C., Rätsch, G., Weigel, D., 2014. Species-wide genetic

incompatibility analysis identifies immune genes as hot spots of deleterious epistasis. Cell 159, 1341–1351. https://doi.org/10.1016/j.cell.2014.10.049

Chen, V.B., Arendall, W.B., Headd, J.J., Keedy, D.A., Immormino, R.M., Kapral, G.J., Murray, L.W., Richardson, J.S., Richardson, D.C., 2010. MolProbity: all-atom structure validation for macromolecular crystallography. Acta Crystallogr D Biol Crystallogr 66, 12–21. https://doi.org/10.1107/S0907444909042073

Costanzo, S., Jia, Y., 2010. Sequence variation at the rice blast resistance gene Pi-km locus: Implications for the development of allele specific markers. Plant Science 178, 523–530. https://doi.org/10.1016/j.plantsci.2010.02.014

De la Concepcion, J.C., Franceschetti, M., MacLean, D., Terauchi, R., Kamoun, S., Banfield, M.J., 2019. Protein engineering expands the effector recognition profile of a rice NLR immune receptor. eLife 8, e47713. https://doi.org/10.7554/eLife.47713

De la Concepcion, J.C., Franceschetti, M., Maqbool, A., Saitoh, H., Terauchi, R., Kamoun, S., Banfield, M.J., 2018. Polymorphic residues in rice NLRs expand binding and response to effectors of the blast pathogen. Nature Plants 4, 576–585. https://doi.org/10.1038/s41477-018-0194-x

De la Concepcion, J.C., Fujisaki, K., Bentham, A.R., Mireles, N.C., Hernandez, V.S. de M., Shimizu, M., Lawson, D.M., Kamoun, S., Terauchi, R., Banfield, M.J., 2022. Binding of a blast fungus Zinc-finger fold effector to a hydrophobic pocket in the host exocyst subunit Exo70 modulates immune recognition in rice. https://doi.org/10.1101/2022.06.18.496527

De la Concepcion, J.C., Maidment, J.H.R., Longya, A., Xiao, G., Franceschetti, M., Banfield, M.J., 2021a. The allelic rice immune receptor Pikh confers extended resistance to strains of the blast fungus through a single polymorphism in the effector binding interface. PLOS Pathogens 17, e1009368. https://doi.org/10.1371/journal.ppat.1009368

De la Concepcion, J.C., Vega Benjumea, J., Bialas, A., Terauchi, R., Kamoun, S., Banfield, M.J., 2021b. Functional diversification gave rise to allelic specialization in a rice NLR immune receptor pair. eLife 10, e71662. https://doi.org/10.7554/eLife.71662

Emsley, P., Cowtan, K., 2004. Coot: model-building tools for molecular graphics. Acta Crystallogr D Biol Crystallogr 60, 2126–2132. https://doi.org/10.1107/S0907444904019158

Engler, C., Youles, M., Gruetzner, R., Ehnert, T.-M., Werner, S., Jones, J.D.G., Patron, N.J., Marillonnet, S., 2014. A Golden Gate Modular Cloning Toolbox for Plants. ACS Synth. Biol. 3, 839–843. https://doi.org/10.1021/sb4001504

Fridy, P.C., Li, Y., Keegan, S., Thompson, M.K., Nudelman, I., Scheid, J.F., Oeffinger, M., Nussenzweig, M.C., Fenyö, D., Chait, B.T., Rout, M.P., 2014. A robust pipeline for rapid production of versatile nanobody repertoires. Nat Methods 11, 1253–1260. https://doi.org/10.1038/nmeth.3170

973 Feehan, J.M., Castel, B., Bentham, A.R., Jones, J.D., 2020. Plant NLRs get by with a little help
974 from their friends. Curr Opin Plant Biol 56, 99–108.
975 https://doi.org/10.1016/j.pbi.2020.04.006

976 Fujisaki, K., Abe, Y., Kanzaki, E., Ito, K., Utsushi, H., Saitoh, H., Białas, A., Banfield, M.J.,
977 Kamoun, S., Terauchi, R., 2017. An unconventional NOI/RIN4 domain of a rice NLR
978 protein binds host EXO70 protein to confer fungal immunity.
979 https://doi.org/10.1101/239400

980 Guo, L., Cesari, S., de Guillen, K., Chalvon, V., Mammri, L., Ma, M., Meusnier, I., Bonnot, F.,
981 Padilla, A., Peng, Y.-L., Liu, J., Kroj, T., 2018. Specific recognition of two MAX
982 effectors by integrated HMA domains in plant immune receptors involves distinct
983 binding surfaces. Proc. Natl. Acad. Sci. U.S.A. 115, 11637–11642.
984 https://doi.org/10.1073/pnas.1810705115

985 Ho, J., Tumkaya, T., Aryal, S., Choi, H., Claridge-Chang, A., 2019. Moving beyond P values:
986 data analysis with estimation graphics. Nat Methods 16, 565–566.
987 https://doi.org/10.1038/s41592-019-0470-3

988 Jones, J.D.G., Vance, R.E., Dangl, J.L., 2016. Intracellular innate immune surveillance devices
989 in plants and animals. Science 354, aaf6395. https://doi.org/10.1126/science.aaf6395

990 Jumper, J., Evans, R., Pritzel, A., Green, T., Figurnov, M., Ronneberger, O.,
991 Tunyasuvunakool, K., Bates, R., Žídek, A., Potapenko, A., Bridgland, A., Meyer, C.,
992 Kohl, S.A.A., Ballard, A.J., Cowie, A., Romera-Paredes, B., Nikolov, S., Jain, R., Adler,
993 J., Back, T., Petersen, S., Reiman, D., Clancy, E., Zielinski, M., Steinegger, M.,
994 Pacholska, M., Berghammer, T., Bodenstein, S., Silver, D., Vinyals, O., Senior, A.W.,
995 Kavukcuoglu, K., Kohli, P., Hassabis, D., 2021. Highly accurate protein structure
996 prediction with AlphaFold. Nature 596, 583–589. https://doi.org/10.1038/s41586-
997 021-03819-2

998 Kanzaki, H., Yoshida, K., Saitoh, H., Fujisaki, K., Hirabuchi, A., Alaux, L., Fournier, E.,
999 Tharreau, D., Terauchi, R., 2012. Arms race co-evolution of Magnaporthe oryzae
1000 AVR-Pik and rice Pik genes driven by their physical interactions. Plant J 72, 894–907.
1001 https://doi.org/10.1111/j.1365-313X.2012.05110.x

1002 Kourelis, J., Adachi, H., 2022. Activation and Regulation of NLR Immune Receptor
1003 Networks. Plant and Cell Physiology pcac116. https://doi.org/10.1093/pcp/pcac116

1004 Kourelis, J., Marchal, C., Posbeyikian, A., Harant, A., Kamoun, S., 2023. NLR immune
1005 receptor–nanobody fusions confer plant disease resistance. Science 379, 934–939.
1006 https://doi.org/10.1126/science.abn4116

1007 Krissinel, E., Henrick, K., 2007. Inference of macromolecular assemblies from crystalline
1008 state. J Mol Biol 372, 774–797. https://doi.org/10.1016/j.jmb.2007.05.022

1009 Kroj, T., Chanclud, E., Michel-Romiti, C., Grand, X., Morel, J.-B., 2016. Integration of decoy
1010 domains derived from protein targets of pathogen effectors into plant immune
1011 receptors is widespread. New Phytologist 210, 618–626.
1012 https://doi.org/10.1111/nph.13869

Le Roux, C., Huet, G., Jauneau, A., Camborde, L., Trémousaygue, D., Kraut, A., Zhou, B., Levaillant, M., Adachi, H., Yoshioka, H., Raffaele, S., Berthomé, R., Couté, Y., Parker, J.E., Deslandes, L., 2015. A Receptor Pair with an Integrated Decoy Converts Pathogen Disabling of Transcription Factors to Immunity. Cell 161, 1074–1088. https://doi.org/10.1016/j.cell.2015.04.025

Liu, Y., Zhang, X., Yuan, G., Wang, D., Zheng, Y., Ma, M., Guo, L., Bhadauria, V., Peng, Y.-L., Liu, J., 2021. A designer rice NLR immune receptor confers resistance to the rice blast fungus carrying noncorresponding avirulence effectors. Proceedings of the National Academy of Sciences 118, e2110751118. https://doi.org/10.1073/pnas.2110751118

Lüdke, D., Yan, Q., Rohmann, P.F.W., Wiermer, M., 2022. NLR we there yet? Nucleocytoplasmic coordination of NLR-mediated immunity. New Phytologist n/a. https://doi.org/10.1111/nph.18359

MacLean, D., 2019. TeamMacLean/besthr: Initial Release. https://doi.org/10.5281/zenodo.3374507

Maidment, J.H.R., Franceschetti, M., Maqbool, A., Saitoh, H., Jantasuriyarat, C., Kamoun, S., Terauchi, R., Banfield, M.J., 2021. Multiple variants of the fungal effector AVR-Pik bind the HMA domain of the rice protein OsHIPP19, providing a foundation to engineer plant defense. Journal of Biological Chemistry 296. https://doi.org/10.1016/j.jbc.2021.100371

Maidment, J.H.R., Shimizu, M., Vera, S., Franceschetti, M., Longya, A., Stevenson, C.E.M., Concepcion, J.D. la, Białas, A., Kamoun, S., Terauchi, R., Banfield, M.J., 2022. Effector target-guided engineering of an integrated domain expands the disease resistance profile of a rice NLR immune receptor. https://doi.org/10.1101/2022.06.14.496076

Maqbool, A., Saitoh, H., Franceschetti, M., Stevenson, C., Uemura, A., Kanzaki, H., Kamoun, S., Terauchi, R., Banfield, M., 2015. Structural basis of pathogen recognition by an integrated HMA domain in a plant NLR immune receptor. eLife 4, e08709. https://doi.org/10.7554/eLife.08709

Marchal, C., Michalopoulou, V.A., Zou, Z., Cevik, V., Sarris, P.F., 2022. Show me your ID: NLR immune receptors with integrated domains in plants. Essays in Biochemistry EBC20210084. https://doi.org/10.1042/EBC20210084

Maruta, N., Burdett, H., Lim, B.Y.J., Hu, X., Desa, S., Manik, M.K., Kobe, B., 2022. Structural basis of NLR activation and innate immune signalling in plants. Immunogenetics 74, 5–26. https://doi.org/10.1007/s00251-021-01242-5

McCoy, A.J., Grosse-Kunstleve, R.W., Adams, P.D., Winn, M.D., Storoni, L.C., Read, R.J., 2007. Phaser crystallographic software. J Appl Crystallogr 40, 658–674. https://doi.org/10.1107/S0021889807021206

Mirdita, M., Schütze, K., Moriwaki, Y., Heo, L., Ovchinnikov, S., Steinegger, M., 2022. ColabFold: making protein folding accessible to all. Nat Methods 19, 679–682. https://doi.org/10.1038/s41592-022-01488-1

1053 Monteiro, F., Nishimura, M.T., 2018. Structural, Functional, and Genomic Diversity of Plant
1054 NLR Proteins: An Evolved Resource for Rational Engineering of Plant Immunity.
1055 Annu. Rev. Phytopathol. 56, 243–267. https://doi.org/10.1146/annurev-phyto-
1056 080417-045817

1057 Mukhi, N., Brown, H., Gorenkin, D., Ding, P., Bentham, A.R., Jones, J.D.G., Banfield, M.J.,
1058 2021. Perception of structurally distinct effectors by the integrated WRKY domain of
1059 a plant immune receptor. https://doi.org/10.1101/2021.07.28.454147

1060 Murshudov, G.N., Vagin, A.A., Dodson, E.J., 1997. Refinement of macromolecular structures
1061 by the maximum-likelihood method. Acta Crystallogr D Biol Crystallogr 53, 240–255.
1062 https://doi.org/10.1107/S0907444996012255

1063 Ordon, J., Martin, P., Erickson, J.L., Ferik, F., Balcke, G., Bonas, U., Stuttmann, J., 2021.
1064 Disentangling cause and consequence: genetic dissection of the DANGEROUS MIX2
1065 risk locus, and activation of the DM2h NLR in autoimmunity. The Plant Journal 106,
1066 1008–1023. https://doi.org/10.1111/tpj.15215

1067 Ortiz, D., de Guillen, K., Cesari, S., Chalvon, V., Gracy, J., Padilla, A., Kroj, T., 2017.
1068 Recognition of the Magnaporthe oryzae Effector AVR-Pia by the Decoy Domain of
1069 the Rice NLR Immune Receptor RGA5[OPEN]. Plant Cell 29, 156–168.
1070 https://doi.org/10.1105/tpc.16.00435

1071 Outram, M.A., Figueroa, M., Sperschneider, J., Williams, S.J., Dodds, P.N., 2022. Seeing is
1072 believing: Exploiting advances in structural biology to understand and engineer
1073 plant immunity. Current Opinion in Plant Biology 67, 102210.
1074 https://doi.org/10.1016/j.pbi.2022.102210

1075 Pettersen, E.F., Goddard, T.D., Huang, C.C., Meng, E.C., Couch, G.S., Croll, T.I., Morris, J.H.,
1076 Ferrin, T.E., 2021. UCSF ChimeraX: Structure visualization for researchers, educators,
1077 and developers. Protein Sci 30, 70–82. https://doi.org/10.1002/pro.3943

1078 Sarris, P.F., Cevik, V., Dagdas, G., Jones, J.D.G., Krasileva, K.V., 2016. Comparative analysis
1079 of plant immune receptor architectures uncovers host proteins likely targeted by
1080 pathogens. BMC Biology 14, 8. https://doi.org/10.1186/s12915-016-0228-7

1081 Studier, F.W., 2005. Protein production by auto-induction in high-density shaking cultures.
1082 Protein Expression and Purification 41, 207–234.
1083 https://doi.org/10.1016/j.pep.2005.01.016

1084 Sugihara, Y., Abe, Y., Takagi, H., Abe, A., Shimizu, M., Ito, K., Kanzaki, E., Oikawa, K.,
1085 Kourelis, J., Langner, T., Win, J., Białas, A., Lüdke, D., Chuma, I., Saitoh, H.,
1086 Kobayashi, M., Zheng, S., Tosa, Y., Banfield, M.J., Kamoun, S., Terauchi, R., Fujisaki,
1087 K., 2022. Tangled gene-for-gene interactions mediate co-evolution of the rice NLR
1088 immune receptor Pik and blast fungus effector proteins.
1089 https://doi.org/10.1101/2022.07.19.500555

1090 Rothbauer, U., Zolghadr, K., Tillib, S., Nowak, D., Schermelleh, L., Gahl, A., Backmann, N.,
1091 Conrath, K., Muyldermans, S., Cardoso, M.C., Leonhardt, H., 2006. Targeting and

tracing antigens in live cells with fluorescent nanobodies. Nat Methods 3, 887–889. https://doi.org/10.1038/nmeth953

Takken, F.L.W., Goverse, A., 2012. How to build a pathogen detector: structural basis of NB-LRR function. Curr Opin Plant Biol 15, 375–384. https://doi.org/10.1016/j.pbi.2012.05.001

Automatic citation updates are disabled. To see the bibliography, click Refresh in the Zotero tab.Tran, D.T.N., Chung, E.-H., Habring-Müller, A., Demar, M., Schwab, R., Dangl, J.L., Weigel, D., Chae, E., 2017. Activation of a Plant NLR Complex through Heteromeric Association with an Autoimmune Risk Variant of Another NLR. Current Biology 27, 1148–1160. https://doi.org/10.1016/j.cub.2017.03.018

Varden, F.A., Saitoh, H., Yoshino, K., Franceschetti, M., Kamoun, S., Terauchi, R., Banfield, M.J., 2019. Cross-reactivity of a rice NLR immune receptor to distinct effectors from the rice blast pathogen Magnaporthe oryzae provides partial disease resistance. J Biol Chem 294, 13006–13016. https://doi.org/10.1074/jbc.RA119.007730

Wickham, H., 2016. ggplot2: Elegant Graphics for Data Analysis. Springer-Verlag New York.

Winn, M.D., Ballard, C.C., Cowtan, K.D., Dodson, E.J., Emsley, P., Evans, P.R., Keegan, R.M., Krissinel, E.B., Leslie, A.G.W., McCoy, A., McNicholas, S.J., Murshudov, G.N., Pannu, N.S., Potterton, E.A., Powell, H.R., Read, R.J., Vagin, A., Wilson, K.S., 2011. Overview of the CCP4 suite and current developments. Acta Crystallogr D Biol Crystallogr 67, 235–242. https://doi.org/10.1107/S0907444910045749

Wu, C.-H., Derevnina, L., Kamoun, S., 2018. Receptor networks underpin plant immunity. Science 360, 1300–1301. https://doi.org/10.1126/science.aat2623

Zdrzałek, R., Kamoun, S., Terauchi, R., Saitoh, H., Banfield, M.J., 2020. The rice NLR pair Pikp-1/Pikp-2 initiates cell death through receptor cooperation rather than negative regulation. PLoS One 15, e0238616. https://doi.org/10.1371/journal.pone.0238616

Zhang, X., Liu, Y., Yuan, G., Wang, D., Zhu, T., Wu, X., Ma, M., Guo, L., Guo, H., Bhadauria, V., Liu, J., Peng, Y.-L., 2022. The effector recognition by synthetic sensor NLR receptors requires the concerted action of multiple interfaces within and outside the integrated domain. https://doi.org/10.1101/2022.08.17.504349

Zhang, Z.-M., Ma, K.-W., Gao, L., Hu, Z., Schwizer, S., Ma, W., Song, J., 2017. Mechanism of host substrate acetylation by a YopJ family effector. Nat Plants 3, 17115. https://doi.org/10.1038/nplants.2017.115

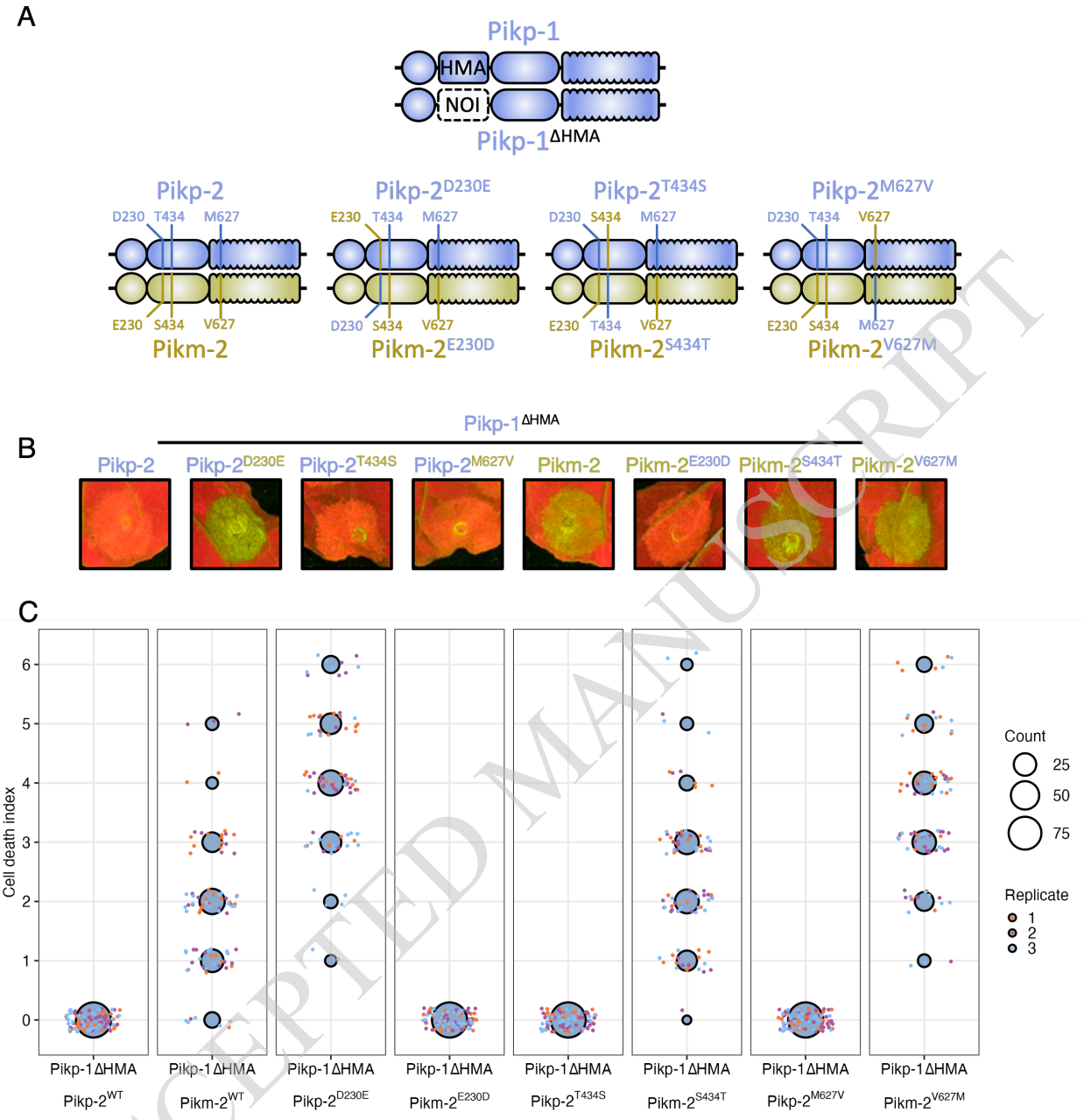

Figure 1. Pik-2 polymorphisms determine Pik-1 HMA domain independent allelic compatibility. A) Schematic diagram highlighting the domain architecture of Pikp-1 and Pikp-1$^{\Delta HMA}$ sensor NLRs (nucleotide-binding leucine-rich repeat receptors) and the polymorphisms between the Pikp-2 and Pikm-2 helper NLRs. **B)** *N. benthamiana* cell death assays of Pikp-1$^{\Delta HMA}$ co-expressed with Pik-2 helpers and mutant variants visualised via ultraviolet light. The HMA (heavy metal-associated) domain of Pikp-1 is not required for effector-independent cell death in *N. benthamiana*; compatibility remains with Pikp-2 but not Pikm-2. Reciprocal D230E and E230D mutations in Pikp-2 and Pikm-2 flip the compatibility of the helper NLRs for Pikp-1$^{\Delta HMA}$. The other polymorphic residues between Pikp-2 and Pikm-2, T434S and M627V, have no effect on

helper compatibility. **C)** Cell death scoring for repeats of Pikp-1$^{\Delta HMA}$ co-expressed with Pikp-2, Pikm-2, and mutants in *N. benthamiana* represented as dot plots. The total number of repeats was spots 75 per sample. For each sample, all the data points are represented as dots with a distinct colour for each of the three biological replicates; these dots are jittered around the cell death score for visualisation purposes. The size of the central dot at each cell death value is proportional to the number of replicates of the sample with that score. Quantification and statistical analysis of these results can be found in **Appendix 1 A**. Details of the NLR mutants used in these experiments can be found in **Supplemental Table S3**.

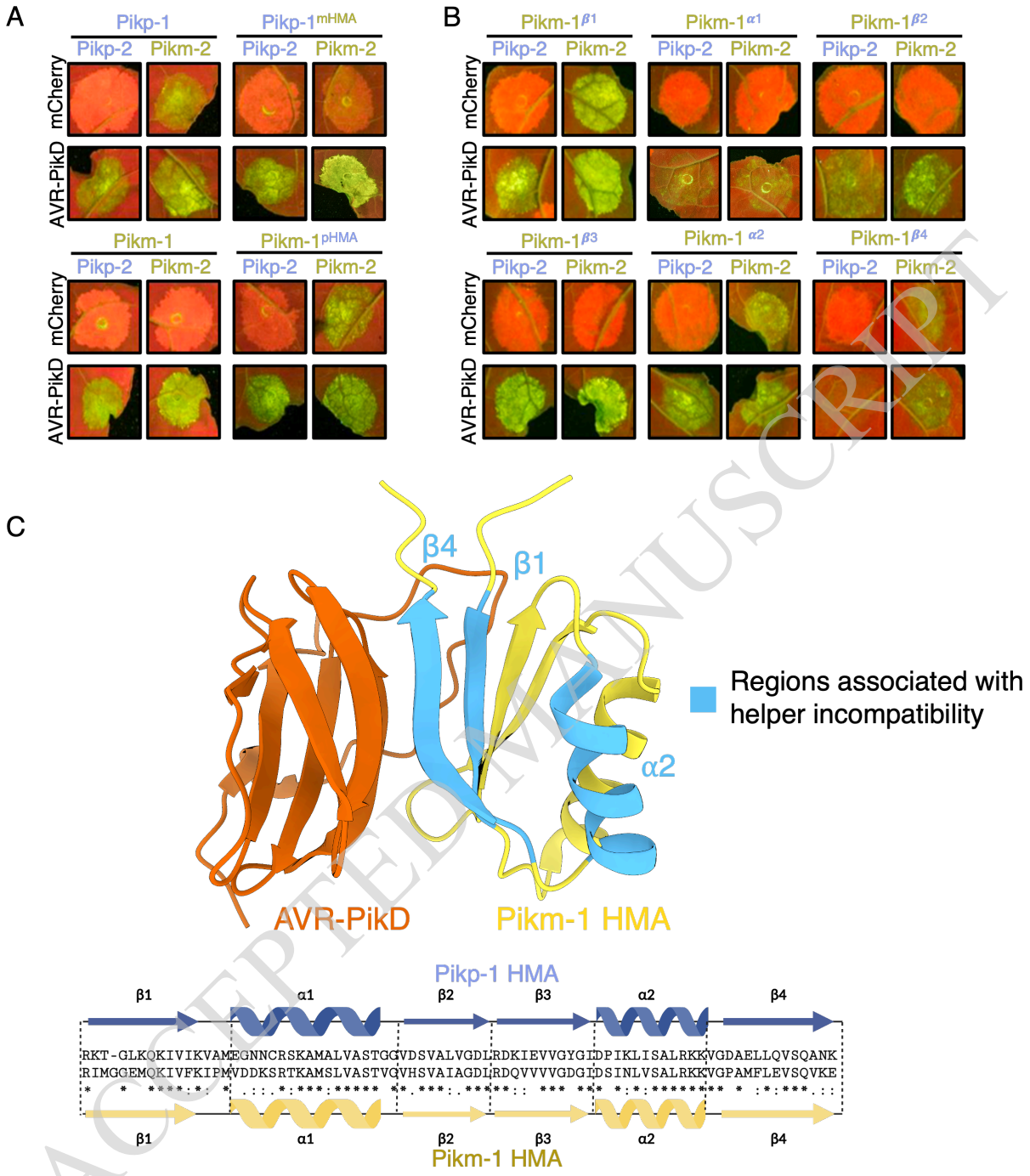

Figure 2. The HMA domain of Pik-1 is important for compatibility with Pik-2 helpers. A) Co-expression of Pikp-1 with Pikm-2 triggers effector-independent cell death in *N. benthamiana.* Integration of the Pikm-1 HMA into Pikp-1 facilitates Pikp-1 compatibility with Pikm-2, whereas incorporation of the Pikp-1 HMA into Pikm-1 abolishes compatibility with Pikm-2. Quantification and statistical analysis of these results are shown in **Figure S1 A, Appendix 1 B. B)** Incompatibility of the Pikp-1 with Pikm-2 in *N. benthamiana* is linked to the α2 helix, β1, and β4 strands of the HMA (heavy metal-associated) domain, with Pikm-1 HMA chimeras carrying

the Pikp-1 secondary structure elements resulting in effector-independent cell death when co-expressed with Pikm-2. Quantification and statistical analysis of these results can be found in **Figure S1 B, Appendix 1 C. C)** Some regions of the HMA domain that are involved in sensor/helper incompatibility (red) are shared with the AVR-Pik binding interface (PDB ID: 6FU9). Details of the NLR mutants used in these experiments can be found in **Supplemental Table S3**.

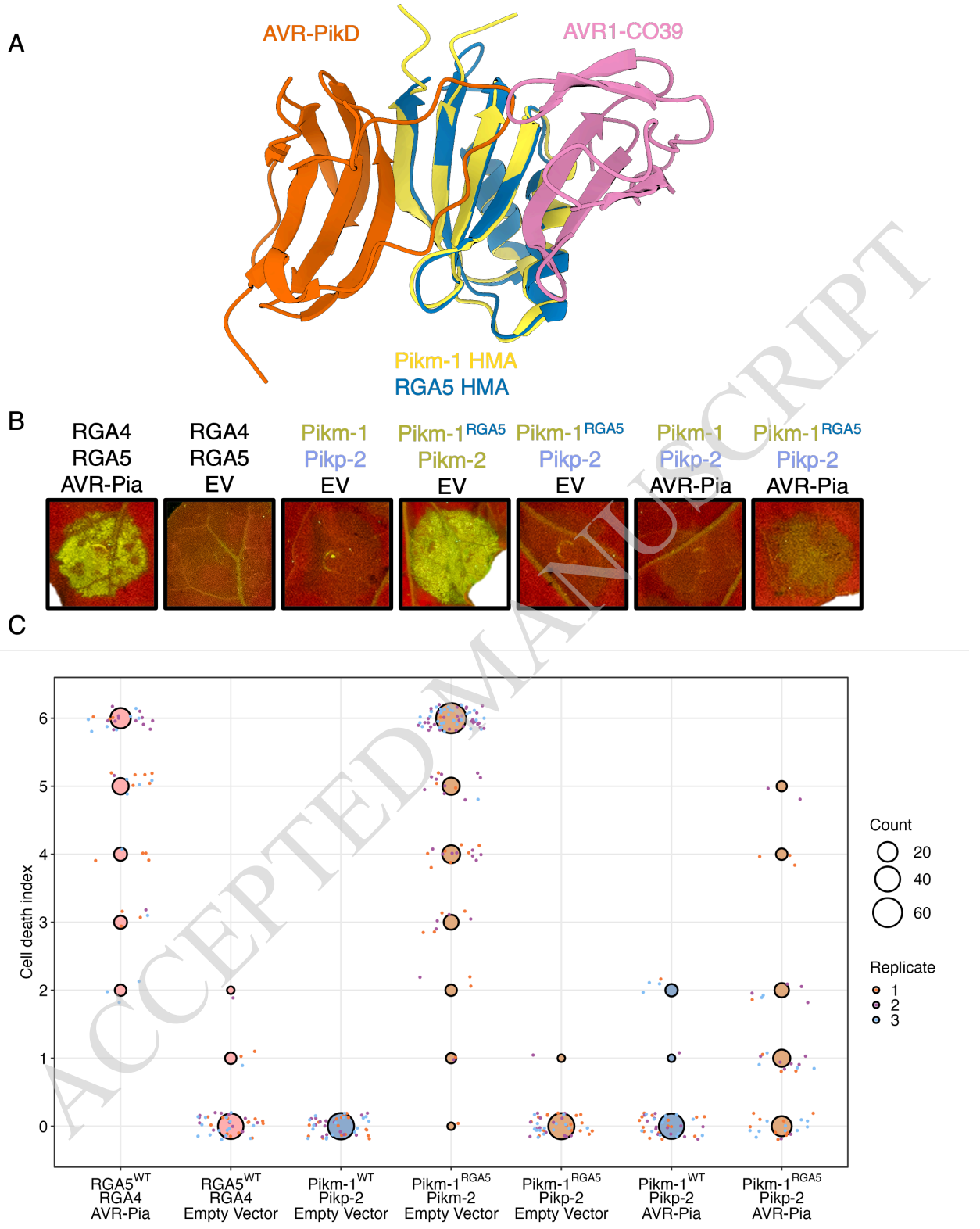

Figure 3. Autoactivity following integration of the RGA5 HMA domain into Pikm-1 is relieved by allelic mismatch with Pikp-2, but only weakly responds to AVR-Pia. A) Schematic structural

alignment of the RGA5 HMA (heavy metal-associated) domain (orange; PDB ID: 5ZNG) with the Pikm-1 HMA domain (gold; PBD ID: 6FU9) showing the different binding interfaces of these HMAs for the AVR-Pik (green) and AVR1-CO39 (cyan)/AVR-Pia (not shown) effectors. B) Co-expression of Pikm-1^{RGA5} with Pikp-2 supresses effector independent cell death in the presence of empty vector (EV) control and responds weakly to AVR-Pia. C) Cell death scoring of wildtype (WT) Pikm-1 and Pikm-1^{RGA5} co-expressed with Pikp-2 in *N. benthamiana* represented as dot plots. The total number of repeats was 45 per sample. For each sample, all the data points are represented as dots with a distinct colour for each of the three biological replicates; these dots are jittered around the cell death score for visualisation purposes. The size of the central dot at each cell death value is proportional to the number of replicates of the sample with that score. Statistical analyses of these results are shown in **Appendix 1 G**. Details of the NLR (nucleotide-binding leucine rich repeat receptor) mutants used in these experiments can be found in **Supplemental Table S3**.

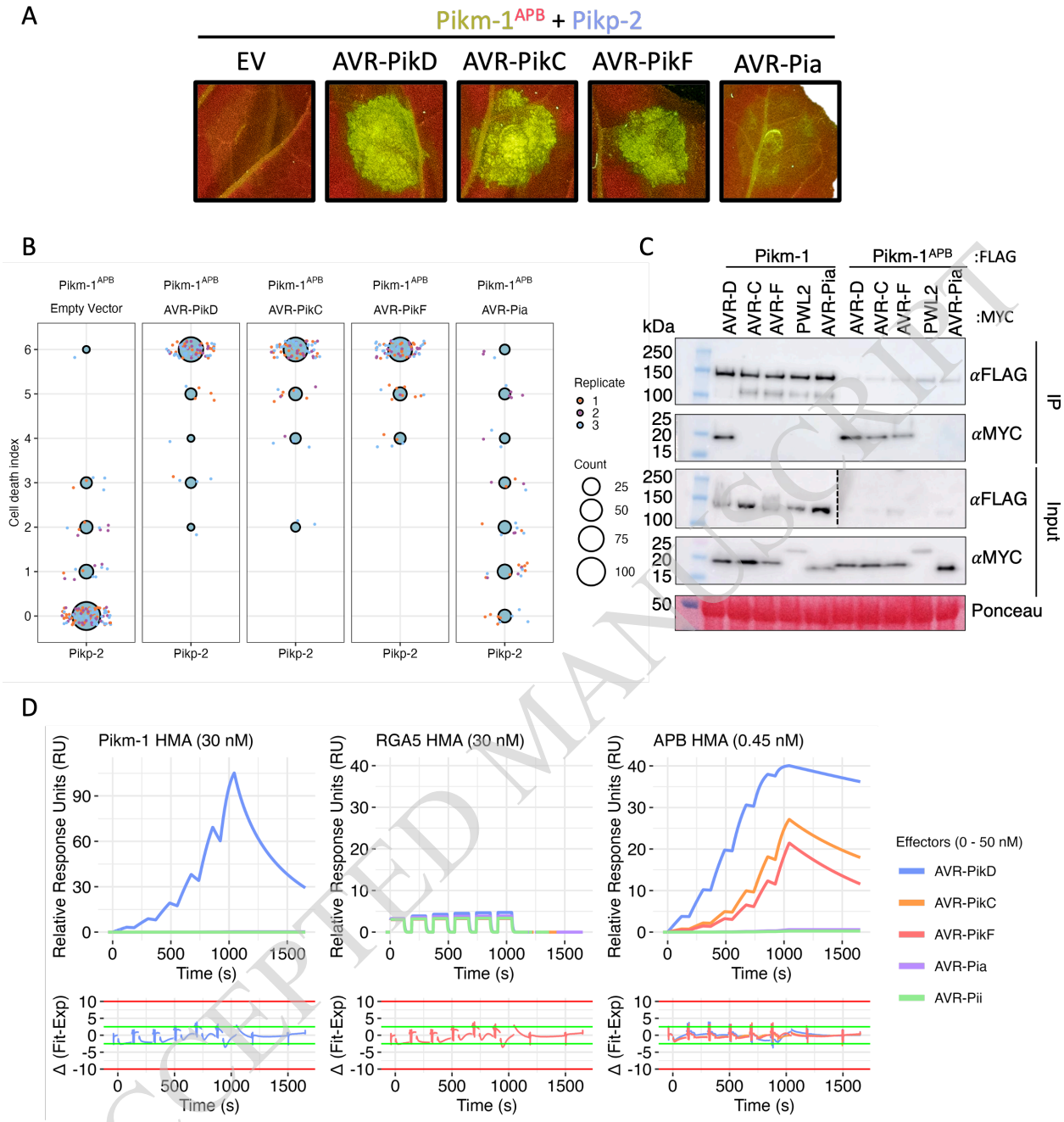

Figure 4. The RGA5 APB mutant binds and recognises AVR-Pik when integrated into Pikm-1. **A)** Pikm-1^{APB} chimera responds to all variants of AVR-Pik tested and activates cell death when co-expressed with Pikp-2 in *N. benthamiana*, but like Pikm-1^{RGA5}, it only weakly responds to AVR-Pia. **B)** Cell death scoring of Pikm-1^{APB} co-expressed with AVR-Pik variants D, C and F in *N. benthamiana* represented as dot plots. The total number of repeats was 80 per sample. For each sample, all the data points are represented as dots with a distinct colour for each of the three biological replicates; these dots are jittered around the cell death score for visualisation purposes. The size of the central dot at each cell death value is proportional to the number of replicates of the sample with that score. Statistical analyses of these results are shown in **Appendix 1 I C)** Co-immunoprecipitation of Pikm-1^{APB} with different MAX (*Magnaporthe* AVRs and ToxB-like)

effectors shows association with AVR-Pik variants, but not AVR-Pia, in planta. Dotted line denotes separate membrane exposures of the same membrane. **D)** Surface plasmon resonance (SPR) sensograms for the interaction of HMA (heavy metal-associated) domains of Pikm-1, RGA5 and RGA5 APB mutant with effectors AVR-PikD, AVR-PikC, AVR-PikF and AVR-Pia. Non-MAX effector AVR-Pii was added as a negative control. Response units for each labelled protein concentration are shown with the residuals plot beneath (SPR acceptance guides as determined by Biacore software are shown as green and red lines in the residuals plots). Concentration of each protein in the assay is indicated next to their corresponding name. Each experiment was repeated a minimum of 3 times, with similar results.

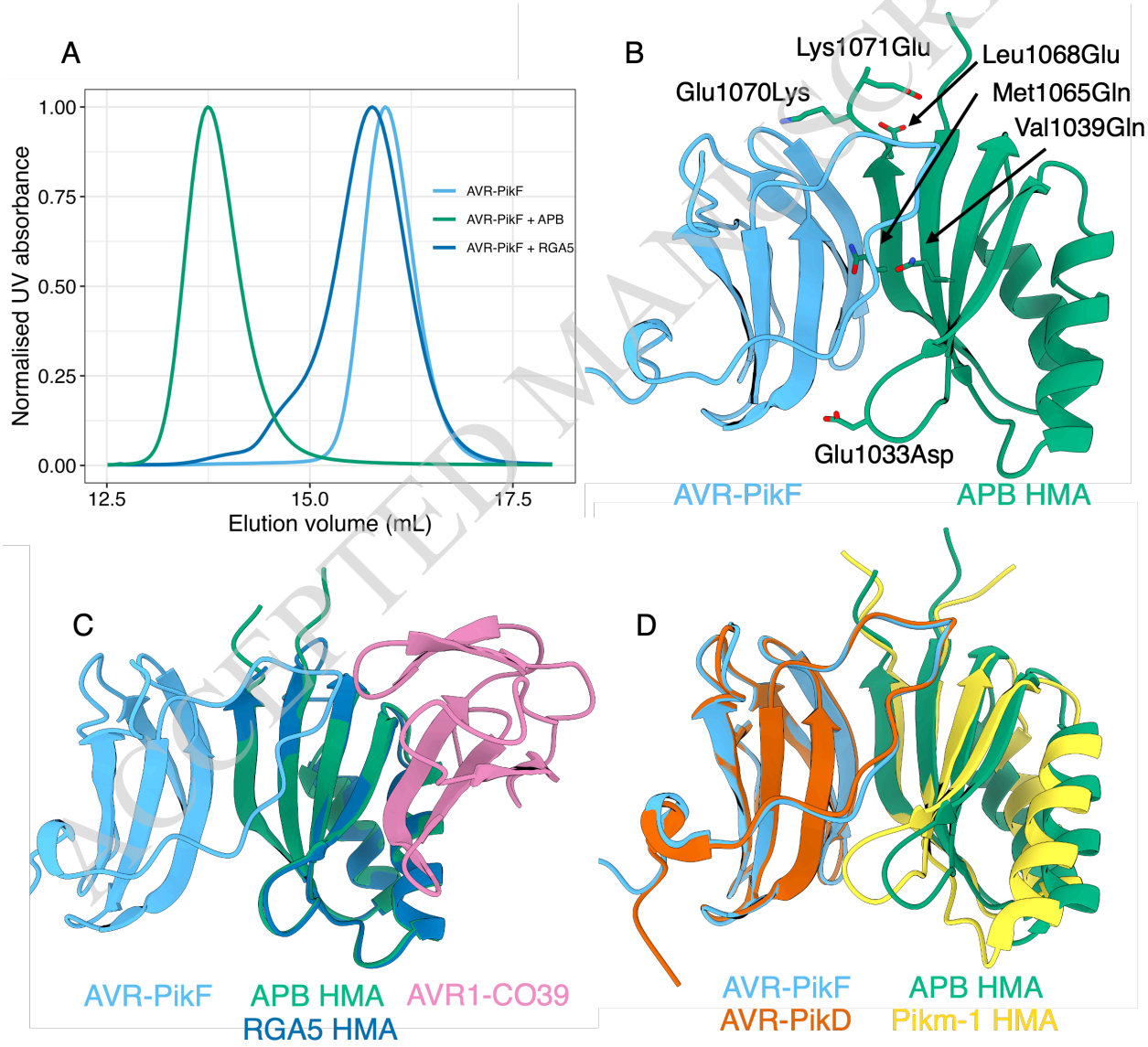

Figure 5. Six mutations in the RGA5 HMA reconstitutes a high affinity AVR-Pik binding interface akin to that of the Pik-1 HMA. A) Analytical size-exclusion chromatography of AVR-

PikF with the RGA5 and APB HMA (heavy metal-associated) proteins. A mixture of AVR-PikF and APB HMA (red) elutes earlier than a mixture of RGA5 and AVR-PikF (orange) or AVR-PikF alone (green), indicative of complex formation between AVR-PikF and the APB HMA. **B)** The crystal structure of AVR-PikF in complex with the RGA5 APB HMA mutant (PDB: 8B2R). Mutations in RGA5, guided by the structure of the OsHIPP19/AVR-PikF complex, are shown forming contacts with AVR-PikF and are labelled. **C)** Superimposition of the crystal structures of the APB/AVR-PikF complex with the RGA5/AVR1-CO39 complex (PDB ID: 5ZNG) showing the swapped effector-binding interface of the APB HMA compared to the RGA5 HMA. **D)** Superimposition of the APB/AVR-PikF complex with the crystal structure of AVR-PikD bound to the Pikm-1 HMA domain (PDB ID: 6G10), showing the shared effector binding interface in these complexes.

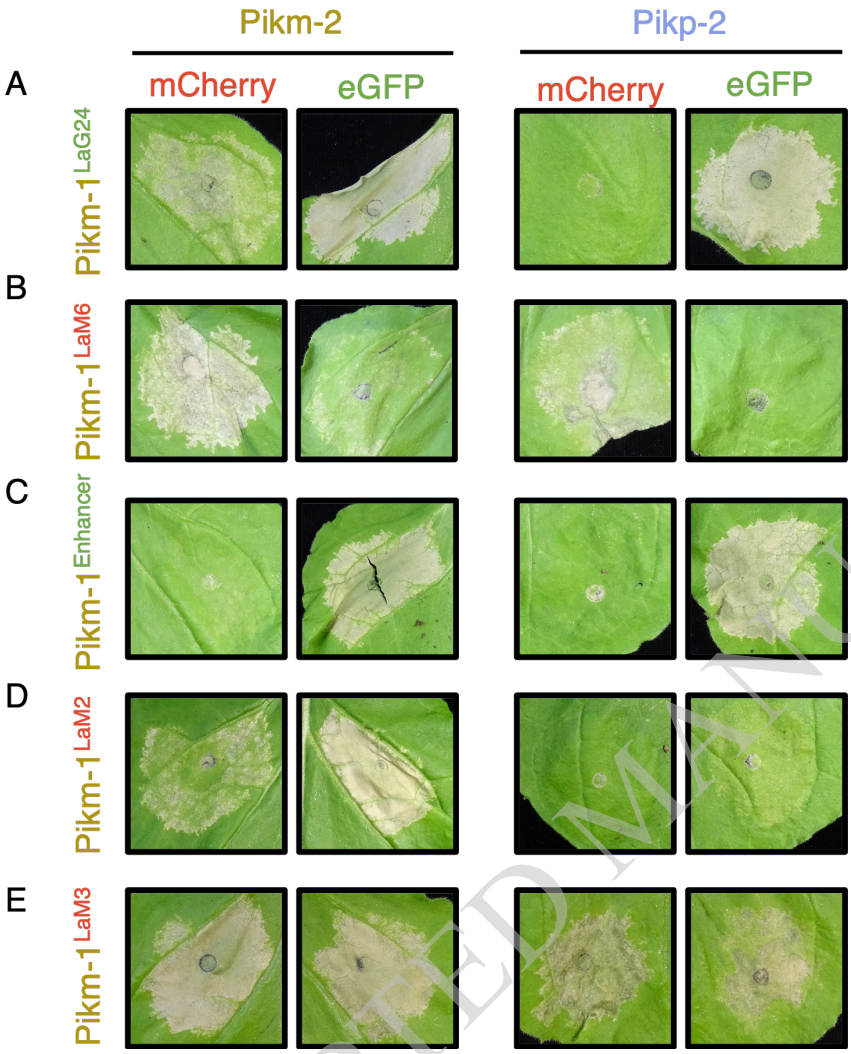

Figure 6. Allelic mismatching of the Pik helper NLRs can be used to alleviate autoactivity from nanobody integration in Pikm-1. Five pikobodies that either respond to the fluorescent protein eGFP (enhanced green fluorescent protein) (Pikm-1^{LaG24} and Pik-1^{Enhancer} indicated by green text) or mCherry (Pikm-1^{LaM2}, Pikm-1^{LaM3} and Pikm-1^{LaM6}, indicated by red text) were tested with the Pikm-2 or Pikp-2 helpers to assess the effect of mismatching on cell death responses in *N. benthamiana*. **A, B)** Pikm-1^{LaG24} and Pikm-1^{LaM6} are autoactive in the presence of Pikm-2, however co-expression with the Pikp-2 helper does not result in autoactivity. Both pikobodies retain ability to respond to their respective fluorescent proteins **C)** Pikm-1^{Enhancer} is not autoactive in the presence of both helpers and can respond to eGFP with equal strength. **D)** Co-expression of Pikm-1^{LaM2} with Pikp-2 alleviates autoactivity observed in the presence of Pikm-2, however response to mCherry is substantially reduced. **E)** Mismatching of the helper alleles is unable to prevent autoactivity induced by the Pikm-1^{LaM3} pikobody. Details of the NLR (nucleotide-binding leucine rich repeat receptor) mutants used in these experiments can be found in **Supplemental Table S3**.

Parsed Citations

Adachi, H., Derevnina, L., Kamoun, S., 2019. NLR singletons, pairs, and networks: evolution, assembly, and regulation of the intracellular immunoreceptor circuitry of plants. Curr Opin Plant Biol 50, 121–131. https://doi.org/10.1016/j.pbi.2019.04.007
Google Scholar: Author Only Title Only Author and Title

Baggs, E., Dagdas, G., Krasileva, K., 2017. NLR diversity, helpers and integrated domains: making sense of the NLR IDentity. Current Opinion in Plant Biology, 38 Biotic interactions 2017 38, 59–67. https://doi.org/10.1016/j.pbi.2017.04.012
Google Scholar: Author Only Title Only Author and Title

Bentham, A.R., De la Concepcion, J.C., Mukhi, N., Zdrzałek, R., Draeger, M., Gorenkin, D., Hughes, R.K., Banfield, M.J., 2020. A molecular roadmap to the plant immune system. JBC 295, 14916–14935. https://doi.org/10.1074/jbc.REV120.010852
Google Scholar: Author Only Title Only Author and Title

Bentham, A.R., Youles, M., Mendel, M.N., Varden, F.A, Concepcion, J.C.D. la, Banfield, M.J., 2021. pOPIN-GG: A resource for modular assembly in protein expression vectors. https://doi.org/10.1101/2021.08.10.455798
Google Scholar: Author Only Title Only Author and Title

Berrow, N.S., Alderton, D., Sainsbury, S., Nettleship, J., Assenberg, R., Rahman, N., Stuart, D.I., Owens, R.J., 2007. A versatile ligation-independent cloning method suitable for high-throughput expression screening applications. Nucleic Acids Res 35, e45. https://doi.org/10.1093/nar/gkm047
Google Scholar: Author Only Title Only Author and Title

Białas, A., Langner, T., Harant, A., Contreras, M.P., Stevenson, C.E., Lawson, D.M., Sklenar, J., Kellner, R., Moscou, M.J., Terauchi, R., Banfield, M.J., Kamoun, S., 2021. Two NLR immune receptors acquired high-affinity binding to a fungal effector through convergent evolution of their integrated domain. eLife 10, e66961. https://doi.org/10.7554/eLife.66961
Google Scholar: Author Only Title Only Author and Title

Białas, A., Zess, E.K., De la Concepcion, J.C., Franceschetti, M., Pennington, H.G., Yoshida, K., Upson, J.L., Chanclud, E., Wu, C.-H., Langner, T., Maqbool, A., Varden, F.A., Derevnina, L., Belhaj, K., Fujisaki, K., Saitoh, H., Terauchi, R., Banfield, M.J., Kamoun, S., 2018. Lessons in Effector and NLR Biology of Plant-Microbe Systems. MPMI 31, 34–45. https://doi.org/10.1094/MPMI-08-17-0196-FI
Google Scholar: Author Only Title Only Author and Title

Bomblies, K., Lempe, J., Epple, P., Warthmann, N., Lanz, C., Dangl, J.L., Weigel, D., 2007. Autoimmune response as a mechanism for a Dobzhansky-Muller-type incompatibility syndrome in plants. PLoS Biol 5, e236. https://doi.org/10.1371/journal.pbio.0050236
Google Scholar: Author Only Title Only Author and Title

Burdett, H., Kobe, B., Anderson, P.A., 2019. Animal NLRs continue to inform plant NLR structure and function. Archives of Biochemistry and Biophysics, Inflammasomes: Intracellular mediators of immune defence 670, 58–68. https://doi.org/10.1016/j.abb.2019.05.001
Google Scholar: Author Only Title Only Author and Title

Calvo-Baltanás, V., Wang, J., Chae, E., 2021. Hybrid Incompatibility of the Plant Immune System: An Opposite Force to Heterosis Equilibrating Hybrid Performances. Frontiers in Plant Science 11.
Google Scholar: Author Only Title Only Author and Title

Cesari, S., 2018. Multiple strategies for pathogen perception by plant immune receptors. New Phytologist 219, 17–24. https://doi.org/10.1111/nph.14877
Google Scholar: Author Only Title Only Author and Title

Cesari, S., Bernoux, M., Moncuquet, P., Kroj, T., Dodds, P.N., 2014. A novel conserved mechanism for plant NLR protein pairs: the "integrated decoy" hypothesis. Front Plant Sci 5, 606. https://doi.org/10.3389/fpls.2014.00606
Google Scholar: Author Only Title Only Author and Title

Cesari, S., Thilliez, G., Ribot, C., Chalvon, V., Michel, C., Jauneau, A., Rivas, S., Alaux, L., Kanzaki, H., Okuyama, Y., Morel, J.-B., Fournier, E., Tharreau, D., Terauchi, R., Kroj, T., 2013. The Rice Resistance Protein Pair RGA4/RGA5 Recognizes the Magnaporthe oryzae Effectors AVR-Pia and AVR1-CO39 by Direct Binding. The Plant Cell 25, 1463–1481. https://doi.org/10.1105/tpc.112.107201
Google Scholar: Author Only Title Only Author and Title

Cesari, S., Xi, Y., Declerck, N., Chalvon, V., Mammri, L., Pugnière, M., Henriquet, C., de Guillen, K., Chochois, V., Padilla, A., Kroj, T., 2022. New recognition specificity in a plant

homo immune receptor by molecular engineering of its integrated domain. Nat Commun 13, 1524. https://doi.org/10.1038/s41467-022-29196-6
Google Scholar: Author Only Title Only Author and Title

Chae, E., Bomblies, K., Kim, S.-T., Karelina, D., Zaidem, M., Ossowski, S., Martín-Pizarro, C., Laitinen, R.A.E., Rowan, B.A., Tenenboim, H., Lechner, S., Demar, M., Habring-Müller, A., Lanz, C., Rätsch, G., Weigel, D., 2014. Species-wide genetic

incompatibility analysis identifies immune genes as hot spots of deleterious epistasis. Cell 159, 1341–1351. https://doi.org/10.1016/j.cell.2014.10.049
Google Scholar: Author Only Title Only Author and Title

Chen, V.B., Arendall, W.B., Headd, J.J., Keedy, D.A., Immormino, R.M., Kapral, G.J., Murray, L.W., Richardson, J.S., Richardson, D.C., 2010. MolProbity: all-atom structure validation for macromolecular crystallography. Acta Crystallogr D Biol Crystallogr 66, 12–21. https://doi.org/10.1107/S0907444909042073
Google Scholar: Author Only Title Only Author and Title

Costanzo, S., Jia, Y., 2010. Sequence variation at the rice blast resistance gene Pi-km locus: Implications for the development of allele specific markers. Plant Science 178, 523–530. https://doi.org/10.1016/j.plantsci.2010.02.014
Google Scholar: Author Only Title Only Author and Title

De la Concepcion, J.C., Franceschetti, M., MacLean, D., Terauchi, R., Kamoun, S., Banfield, M.J., 2019. Protein engineering expands the effector recognition profile of a rice NLR immune receptor. eLife 8, e47713. https://doi.org/10.7554/eLife.47713
Google Scholar: Author Only Title Only Author and Title

De la Concepcion, J.C., Franceschetti, M., Maqbool, A., Saitoh, H., Terauchi, R., Kamoun, S., Banfield, M.J., 2018. Polymorphic residues in rice NLRs expand binding and response to effectors of the blast pathogen. Nature Plants 4, 576–585. https://doi.org/10.1038/s41477-018-0194-x
Google Scholar: Author Only Title Only Author and Title

De la Concepcion, J.C., Fujisaki, K., Bentham, A.R., Mireles, N.C., Hernandez, V.S. de M., Shimizu, M., Lawson, D.M., Kamoun, S., Terauchi, R., Banfield, M.J., 2022. Binding of a blast fungus Zinc-finger fold effector to a hydrophobic pocket in the host exocyst subunit Exo70 modulates immune recognition in rice. https://doi.org/10.1101/2022.06.18.496527
Google Scholar: Author Only Title Only Author and Title

De la Concepcion, J.C., Maidment, J.H.R., Longya, A., Xiao, G., Franceschetti, M., Banfield, M.J., 2021a. The allelic rice immune receptor Pikh confers extended resistance to strains of the blast fungus through a single polymorphism in the effector binding interface. PLOS Pathogens 17, e1009368. https://doi.org/10.1371/journal.ppat.1009368
Google Scholar: Author Only Title Only Author and Title

De la Concepcion, J.C., Vega Benjumea, J., Bialas, A., Terauchi, R., Kamoun, S., Banfield, M.J., 2021b. Functional diversification gave rise to allelic specialization in a rice NLR immune receptor pair. eLife 10, e71662. https://doi.org/10.7554/eLife.71662
Google Scholar: Author Only Title Only Author and Title

Emsley, P., Cowtan, K., 2004. Coot: model-building tools for molecular graphics. Acta Crystallogr D Biol Crystallogr 60, 2126–2132. https://doi.org/10.1107/S0907444904019158
Google Scholar: Author Only Title Only Author and Title

Engler, C., Youles, M., Gruetzner, R., Ehnert, T.-M., Werner, S., Jones, J.D.G., Patron, N.J., Marillonnet, S., 2014. A Golden Gate Modular Cloning Toolbox for Plants. ACS Synth. Biol. 3, 839–843. https://doi.org/10.1021/sb4001504
Google Scholar: Author Only Title Only Author and Title

Fridy, P.C., Li, Y., Keegan, S., Thompson, M.K., Nudelman, I., Scheid, J.F., Oeffinger, M., Nussenzweig, M.C., Fenyö, D., Chait, B.T., Rout, M.P., 2014. A robust pipeline for rapid production of versatile nanobody repertoires. Nat Methods 11, 1253–1260. https://doi.org/10.1038/nmeth.3170
Google Scholar: Author Only Title Only Author and Title

Feehan, J.M., Castel, B., Bentham, A.R., Jones, J.D., 2020. Plant NLRs get by with a little help from their friends. Curr Opin Plant Biol 56, 99–108. https://doi.org/10.1016/j.pbi.2020.04.006
Google Scholar: Author Only Title Only Author and Title

Fujisaki, K., Abe, Y., Kanzaki, E., Ito, K., Utsushi, H., Saitoh, H., Białas, A., Banfield, M.J., Kamoun, S., Terauchi, R., 2017. An unconventional NOI/RIN4 domain of a rice NLR protein binds host EXO70 protein to confer fungal immunity. https://doi.org/10.1101/239400
Google Scholar: Author Only Title Only Author and Title

Guo, L., Cesari, S., de Guillen, K., Chalvon, V., Mammri, L., Ma, M., Meusnier, I., Bonnot, F., Padilla, A., Peng, Y.-L., Liu, J., Kroj, T., 2018. Specific recognition of two MAX effectors by integrated HMA domains in plant immune receptors involves distinct binding surfaces. Proc. Natl. Acad. Sci. U.S.A. 115, 11637–11642. https://doi.org/10.1073/pnas.1810705115
Google Scholar: Author Only Title Only Author and Title

Ho, J., Tumkaya, T., Aryal, S., Choi, H., Claridge-Chang, A., 2019. Moving beyond P values: data analysis with estimation graphics. Nat Methods 16, 565–566. https://doi.org/10.1038/s41592-019-0470-3
Google Scholar: Author Only Title Only Author and Title

Jones, J.D.G., Vance, R.E., Dangl, J.L., 2016. Intracellular innate immune surveillance devices in plants and animals. Science 354, aaf6395. https://doi.org/10.1126/science.aaf6395
Google Scholar: Author Only Title Only Author and Title

Jumper, J., Evans, R., Pritzel, A., Green, T., Figurnov, M., Ronneberger, O., Tunyasuvunakool, K., Bates, R., Žídek, A., Potapenko, A., Bridgland, A., Meyer, C., Kohl, S.A.A., Ballard, A.J., Cowie, A., Romera-Paredes, B., Nikolov, S., Jain, R., Adler, J., Back, T., Petersen, S., Reiman, D., Clancy, E., Zielinski, M., Steinegger, M., Pacholska, M., Berghammer, T., Bodenstein, S., Silver, D., Vinyals, O., Senior, A.W., Kavukcuoglu, K., Kohli, P., Hassabis, D., 2021. Highly accurate protein structure prediction with AlphaFold. Nature 596, 583–589. https://doi.org/10.1038/s41586-021-03819-2
Google Scholar: Author Only Title Only Author and Title

Kanzaki, H., Yoshida, K., Saitoh, H., Fujisaki, K., Hirabuchi, A., Alaux, L., Fournier, E., Tharreau, D., Terauchi, R., 2012. Arms race co-evolution of Magnaporthe oryzae AVR-Pik and rice Pik genes driven by their physical interactions. Plant J 72, 894–907. https://doi.org/10.1111/j.1365-313X.2012.05110.x
Google Scholar: Author Only Title Only Author and Title

Kourelis, J., Adachi, H., 2022. Activation and Regulation of NLR Immune Receptor Networks. Plant and Cell Physiology pcac116. https://doi.org/10.1093/pcp/pcac116
Google Scholar: Author Only Title Only Author and Title

Kourelis, J., Marchal, C., Posbeyikian, A., Harant, A., Kamoun, S., 2023. NLR immune receptor–nanobody fusions confer plant disease resistance. Science 379, 934–939. https://doi.org/10.1126/science.abn4116
Google Scholar: Author Only Title Only Author and Title

Krissinel, E., Henrick, K., 2007. Inference of macromolecular assemblies from crystalline state. J Mol Biol 372, 774–797. https://doi.org/10.1016/j.jmb.2007.05.022
Google Scholar: Author Only Title Only Author and Title

Kroj, T., Chanclud, E., Michel-Romiti, C., Grand, X., Morel, J.-B., 2016. Integration of decoy domains derived from protein targets of pathogen effectors into plant immune receptors is widespread. New Phytologist 210, 618–626. https://doi.org/10.1111/nph.13869
Google Scholar: Author Only Title Only Author and Title

Le Roux, C., Huet, G., Jauneau, A., Camborde, L., Trémousaygue, D., Kraut, A., Zhou, B., Levaillant, M., Adachi, H., Yoshioka, H., Raffaele, S., Berthomé, R., Couté, Y., Parker, J.E., Deslandes, L., 2015. A Receptor Pair with an Integrated Decoy Converts Pathogen Disabling of Transcription Factors to Immunity. Cell 161, 1074–1088. https://doi.org/10.1016/j.cell.2015.04.025
Google Scholar: Author Only Title Only Author and Title

Liu, Y., Zhang, X., Yuan, G., Wang, D., Zheng, Y., Ma, M., Guo, L., Bhadauria, V., Peng, Y.-L., Liu, J., 2021. A designer rice NLR immune receptor confers resistance to the rice blast fungus carrying noncorresponding avirulence effectors. Proceedings of the National Academy of Sciences 118, e2110751118. https://doi.org/10.1073/pnas.2110751118
Google Scholar: Author Only Title Only Author and Title

Lüdke, D., Yan, Q., Rohmann, P.F.W., Wiermer, M., 2022. NLR we there yet? Nucleocytoplasmic coordination of NLR-mediated immunity. New Phytologist n/a. https://doi.org/10.1111/nph.18359
Google Scholar: Author Only Title Only Author and Title

MacLean, D., 2019. TeamMacLean/besthr: Initial Release. https://doi.org/10.5281/zenodo.3374507
Google Scholar: Author Only Title Only Author and Title

Maidment, J.H.R., Franceschetti, M., Maqbool, A., Saitoh, H., Jantasuriyarat, C., Kamoun, S., Terauchi, R., Banfield, M.J., 2021. Multiple variants of the fungal effector AVR-Pik bind the HMA domain of the rice protein OsHIPP19, providing a foundation to engineer plant defense. Journal of Biological Chemistry 296. https://doi.org/10.1016/j.jbc.2021.100371
Google Scholar: Author Only Title Only Author and Title

Maidment, J.H.R., Shimizu, M., Vera, S., Franceschetti, M., Longya, A., Stevenson, C.E.M., Concepcion, J.D. la, Białas, A., Kamoun, S., Terauchi, R., Banfield, M.J., 2022. Effector target-guided engineering of an integrated domain expands the disease resistance profile of a rice NLR immune receptor. https://doi.org/10.1101/2022.06.14.496076
Google Scholar: Author Only Title Only Author and Title

Maqbool, A., Saitoh, H., Franceschetti, M., Stevenson, C., Uemura, A., Kanzaki, H., Kamoun, S., Terauchi, R., Banfield, M., 2015. Structural basis of pathogen recognition by an integrated HMA domain in a plant NLR immune receptor. eLife 4, e08709. https://doi.org/10.7554/eLife.08709
Google Scholar: Author Only Title Only Author and Title

Marchal, C., Michalopoulou, V.A., Zou, Z., Cevik, V., Sarris, P.F., 2022. Show me your ID: NLR immune receptors with integrated domains in plants. Essays in Biochemistry EBC20210084. https://doi.org/10.1042/EBC20210084
Google Scholar: Author Only Title Only Author and Title

Maruta, N., Burdett, H., Lim, B.Y.J., Hu, X., Desa, S., Manik, M.K., Kobe, B., 2022. Structural basis of NLR activation and innate immune signalling in plants. Immunogenetics 74, 5–26. https://doi.org/10.1007/s00251-021-01242-5
Google Scholar: Author Only Title Only Author and Title

McCoy, A.J., Grosse-Kunstleve, R.W., Adams, P.D., Winn, M.D., Storoni, L.C., Read, R.J., 2007. Phaser crystallographic software. J Appl Crystallogr 40, 658–674. https://doi.org/10.1107/S0021889807021206

Google Scholar: Author Only Title Only Author and Title

Mirdita, M., Schütze, K., Moriwaki, Y., Heo, L., Ovchinnikov, S., Steinegger, M., 2022. ColabFold: making protein folding accessible to all. Nat Methods 19, 679–682. https://doi.org/10.1038/s41592-022-01488-1
Google Scholar: Author Only Title Only Author and Title

Monteiro, F., Nishimura, M.T., 2018. Structural, Functional, and Genomic Diversity of Plant NLR Proteins: An Evolved Resource for Rational Engineering of Plant Immunity. Annu. Rev. Phytopathol. 56, 243–267. https://doi.org/10.1146/annurev-phyto-080417-045817
Google Scholar: Author Only Title Only Author and Title

Mukhi, N., Brown, H., Gorenkin, D., Ding, P., Bentham, A.R., Jones, J.D.G., Banfield, M.J., 2021. Perception of structurally distinct effectors by the integrated WRKY domain of a plant immune receptor. https://doi.org/10.1101/2021.07.28.454147
Google Scholar: Author Only Title Only Author and Title

Murshudov, G.N., Vagin, A.A., Dodson, E.J., 1997. Refinement of macromolecular structures by the maximum-likelihood method. Acta Crystallogr D Biol Crystallogr 53, 240–255. https://doi.org/10.1107/S0907444996012255
Google Scholar: Author Only Title Only Author and Title

Ordon, J., Martin, P., Erickson, J.L., Ferik, F., Balcke, G., Bonas, U., Stuttmann, J., 2021. Disentangling cause and consequence: genetic dissection of the DANGEROUS MIX2 risk locus, and activation of the DM2h NLR in autoimmunity. The Plant Journal 106, 1008–1023. https://doi.org/10.1111/tpj.15215
Google Scholar: Author Only Title Only Author and Title

Ortiz, D., de Guillen, K., Cesari, S., Chalvon, V., Gracy, J., Padilla, A., Kroj, T., 2017. Recognition of the Magnaporthe oryzae Effector AVR-Pia by the Decoy Domain of the Rice NLR Immune Receptor RGA5[OPEN]. Plant Cell 29, 156–168. https://doi.org/10.1105/tpc.16.00435
Google Scholar: Author Only Title Only Author and Title

Outram, M.A., Figueroa, M., Sperschneider, J., Williams, S.J., Dodds, P.N., 2022. Seeing is believing: Exploiting advances in structural biology to understand and engineer plant immunity. Current Opinion in Plant Biology 67, 102210. https://doi.org/10.1016/j.pbi.2022.102210
Google Scholar: Author Only Title Only Author and Title

Pettersen, E.F., Goddard, T.D., Huang, C.C., Meng, E.C., Couch, G.S., Croll, T.I., Morris, J.H., Ferrin, T.E., 2021. UCSF ChimeraX: Structure visualization for researchers, educators, and developers. Protein Sci 30, 70–82. https://doi.org/10.1002/pro.3943
Google Scholar: Author Only Title Only Author and Title

Sarris, P.F., Cevik, V., Dagdas, G., Jones, J.D.G., Krasileva, K.V., 2016. Comparative analysis of plant immune receptor architectures uncovers host proteins likely targeted by pathogens. BMC Biology 14, 8. https://doi.org/10.1186/s12915-016-0228-7
Google Scholar: Author Only Title Only Author and Title

Studier, F.W., 2005. Protein production by auto-induction in high-density shaking cultures. Protein Expression and Purification 41, 207–234. https://doi.org/10.1016/j.pep.2005.01.016
Google Scholar: Author Only Title Only Author and Title

Sugihara, Y., Abe, Y., Takagi, H., Abe, A., Shimizu, M., Ito, K., Kanzaki, E., Oikawa, K., Kourelis, J., Langner, T., Win, J., Białas, A., Lüdke, D., Chuma, I., Saitoh, H., Kobayashi, M., Zheng, S., Tosa, Y., Banfield, M.J., Kamoun, S., Terauchi, R., Fujisaki, K., 2022. Tangled gene-for-gene interactions mediate co-evolution of the rice NLR immune receptor Pik and blast fungus effector proteins. https://doi.org/10.1101/2022.07.19.500555
Google Scholar: Author Only Title Only Author and Title

Rothbauer, U., Zolghadr, K., Tillib, S., Nowak, D., Schermelleh, L., Gahl, A., Backmann, N., Conrath, K., Muyldermans, S., Cardoso, M.C., Leonhardt, H., 2006. Targeting and tracing antigens in live cells with fluorescent nanobodies. Nat Methods 3, 887–889. https://doi.org/10.1038/nmeth953
Google Scholar: Author Only Title Only Author and Title

Takken, F.L.W., Goverse, A., 2012. How to build a pathogen detector: structural basis of NB-LRR function. Curr Opin Plant Biol 15, 375–384. https://doi.org/10.1016/j.pbi.2012.05.001
Google Scholar: Author Only Title Only Author and Title

Automatic citation updates are disabled. To see the bibliography, click Refresh in the Zotero tab.Tran, D.T.N., Chung, E.-H., Habring-Müller, A., Demar, M., Schwab, R., Dangl, J.L., Weigel, D., Chae, E., 2017. Activation of a Plant NLR Complex through Heteromeric Association with an Autoimmune Risk Variant of Another NLR. Current Biology 27, 1148–1160. https://doi.org/10.1016/j.cub.2017.03.018
Google Scholar: Author Only Title Only Author and Title

Varden, F.A., Saitoh, H., Yoshino, K., Franceschetti, M., Kamoun, S., Terauchi, R., Banfield, M.J., 2019. Cross-reactivity of a rice NLR immune receptor to distinct effectors from the rice blast pathogen Magnaporthe oryzae provides partial disease resistance. J Biol Chem 294, 13006–13016. https://doi.org/10.1074/jbc.RA119.007730

Google Scholar: Author Only Title Only Author and Title

Wickham, H., 2016. ggplot2: Elegant Graphics for Data Analysis. Springer-Verlag New York.
Google Scholar: Author Only Title Only Author and Title

Winn, M.D., Ballard, C.C., Cowtan, K.D., Dodson, E.J., Emsley, P., Evans, P.R., Keegan, R.M., Krissinel, E.B., Leslie, A.G.W., McCoy, A., McNicholas, S.J., Murshudov, G.N., Pannu, N.S., Potterton, E.A., Powell, H.R., Read, R.J., Vagin, A., Wilson, K.S., 2011. Overview of the CCP4 suite and current developments. Acta Crystallogr D Biol Crystallogr 67, 235–242. https://doi.org/10.1107/S0907444910045749
Google Scholar: Author Only Title Only Author and Title

Wu, C.-H., Derevnina, L., Kamoun, S., 2018. Receptor networks underpin plant immunity. Science 360, 1300–1301. https://doi.org/10.1126/science.aat2623
Google Scholar: Author Only Title Only Author and Title

Zdrzałek, R., Kamoun, S., Terauchi, R., Saitoh, H., Banfield, M.J., 2020. The rice NLR pair Pikp-1/Pikp-2 initiates cell death through receptor cooperation rather than negative regulation. PLoS One 15, e0238616. https://doi.org/10.1371/journal.pone.0238616
Google Scholar: Author Only Title Only Author and Title

Zhang, X., Liu, Y., Yuan, G., Wang, D., Zhu, T., Wu, X., Ma, M., Guo, L., Guo, H., Bhadauria, V., Liu, J., Peng, Y.-L., 2022. The effector recognition by synthetic sensor NLR receptors requires the concerted action of multiple interfaces within and outside the integrated domain. https://doi.org/10.1101/2022.08.17.504349
Google Scholar: Author Only Title Only Author and Title

Zhang, Z.-M., Ma, K.-W., Gao, L., Hu, Z., Schwizer, S., Ma, W., Song, J., 2017. Mechanism of host substrate acetylation by a YopJ family effector. Nat Plants 3, 17115. https://doi.org/10.1038/nplants.2017.115
Google Scholar: Author Only Title Only Author and Title